Monthly Notices of the ROYAL ASTRONOMICAL SOCIETY

MNRAS **524,** 6181–6197 (2023) https://doi.org/10.1093/mnras/stad2281
Advance Access publication 2023 July 26

On the pollution of white dwarfs by exo-Oort cloud comets

Christopher E. O'Connor [1,2]★ Dong Lai[1,3] and Darryl Z. Seligman[1,3]

[1]*Department of Astronomy and Cornell Center for Astrophysics and Planetary Science, Cornell University, Ithaca, NY 14853, USA*
[2]*Kavli Institute for Theoretical Physics, University of California, Santa Barbara, CA 93106, USA*
[3]*Carl Sagan Institute, Cornell University, Ithaca, NY 14853, USA*

Accepted 2023 July 24. Received 2023 July 19; in original form 2023 June 9

ABSTRACT

A large fraction of white dwarfs (WDs) have metal-polluted atmospheres, which are produced by accreting material from remnant planetary systems. The composition of the accreted debris broadly resembles that of rocky Solar system objects. Volatile-enriched debris with compositions similar to long-period comets (LPCs) is rarely observed. We attempt to reconcile this dearth of volatiles with the premise that exo-Oort clouds (XOCs) occur around a large fraction of planet-hosting stars. We estimate the comet accretion rate from an XOC analytically, adapting the 'loss cone' theory of LPC delivery in the Solar system. We investigate the dynamical evolution of an XOC during late stellar evolution. Using numerical simulations, we show that 1–30 per cent of XOC objects remain bound after anisotropic stellar mass-loss imparting a WD natal kick of $\sim$1 km s^{-1}. We also characterize the surviving comets' distribution function. Surviving planets orbiting a WD can prevent the accretion of XOC comets by the star. A planet's 'dynamical barrier' is effective at preventing comet accretion if the energy kick imparted by the planet exceeds the comet's orbital binding energy. By modifying the loss cone theory, we calculate the amount by which a planet reduces the WD's accretion rate. We suggest that the scarcity of volatile-enriched debris in polluted WDs is caused by an unseen population of 10–100 au scale giant planets acting as barriers to incoming LPCs. Finally, we constrain the amount of volatiles delivered to a planet in the habitable zone of an old, cool WD.

Key words: comets: general – Oort cloud – planets and satellites: dynamical evolution and stability – white dwarfs.

1 INTRODUCTION

The Solar system has two major populations of comets. Long-period comets (period $P \geq 200$ yr; LPCs) have nearly parabolic orbits and isotropic inclinations. They originate from the Oort cloud (OC), a swarm of $\sim 10^{11}$–10^{12} bodies (Oort 1950; Francis 2005; Brasser & Morbidelli 2013; Boe et al. 2019) with a combined mass of $\approx$1–20$M_\oplus$ (Weissman 1996; Fernández & Brunini 2000; Francis 2005; Brasser 2008; Boe et al. 2019) extending up to $\sim 10^5$ au from the Sun. LPCs most likely have a broad distribution of eccentricities, but only those with eccentricity $\simeq$1 are observed entering the inner Solar system. Short-period comets ($P < 200$ yr; SPCs) typically have low inclinations relative to the ecliptic plane. Many come from the trans-Neptunian region (e.g. Duncan & Levison 1997; Levison et al. 2006; Volk & Malhotra 2008), but the Halley-type SPCs may be former OC members captured at shorter periods (Levison, Dones & Duncan 2001; Nesvorný et al. 2017).

The small bodies within the Solar system – including the comets – are believed to be byproducts of the system's formation and subsequent dynamical evolution (see the recent review by Kaib & Volk 2022). Numerous icy planetesimals formed in or beyond the vicinity of the giant planets (when the latter formed, although they have since migrated) and were subsequently expelled by gravitational scattering (e.g. Duncan, Quinn & Tremaine 1987; Hahn & Malhotra 1999; Brasser & Morbidelli 2013; Vokrouhlický, Nesvorný & Dones 2019). Most were ejected into interstellar space, but 1–10 per cent were captured on relatively stable orbits in the OC by external perturbations, such as stellar flybys and the Galactic tide (Hahn & Malhotra 1999; Dones et al. 2004; Brasser, Higuchi & Kaib 2010; Higuchi & Kokubo 2015). Planetesimals expelled from the giant-planet region also populated the Kuiper belt's scattered disc, the main source of SPCs. The existence of extrasolar comet reservoirs is therefore a natural extrapolation from the ubiquity of extrasolar planetary systems with long-period giant planets (Suzuki et al. 2016; Fernandes et al. 2019; Fulton et al. 2021; Poleski et al. 2021). In this work, we focus on extrasolar Oort clouds (XOCs) specifically.

Two lines of evidence suggest exocomets may be common. One comes from rapidly varying spectroscopic absorption features in stellar observations, which are naturally explained by evaporating bodies falling onto their host stars. This occurs most famously in the β Pic system (Ferlet, Hobbs & Vidal-Madjar 1987; Beust, Vidal-Madjar & Ferlet 1991; Pavlenko et al. 2022). The other line of evidence comes from photometric transits of dusty cometary debris (Boyajian et al. 2016; Kiefer et al. 2017; Rappaport et al. 2018; Kennedy et al. 2019; Zieba et al. 2019). The extent to which the observed exocomets are analogous to Solar system comets is unclear (see Strøm et al. 2020 for an introductory review of this topic). The size-frequency distribution of exocomets transiting β Pic is similar to those in the Solar system population (Lecavelier des Etangs et al. 2022). However, relatively little is known about exocometary chemical compositions (e.g. Zuckerman & Song 2012; Matrà et al. 2015; Kral et al. 2017).

★ E-mail: coconnor@astro.cornell.edu

Interstellar interlopers such as 1I/'Oumuamua and 2I/Borisov provide an indirect hint at the existence of XOCs because they may represent the large number of ejected planetesimals implied by XOC formation models (Gaidos, Williams & Kraus 2017; Do, Tucker & Tonry 2018; Gaidos 2018; Moro-Martín 2018, 2019; Portegies Zwart 2021; Jewitt & Seligman 2022; Seligman et al. 2022a). They also add to the available compositional information about exocomets. For example, 2I/Borisov was enriched in CO relative to H_2O, indicative of formation at the CO snowline or beyond (Bodewits et al. 2020; Cordiner et al. 2020; Yang et al. 2021). However, absent spectroscopic measurements of interstellar comets in the inner Solar system, measuring compositional abundances of XOCs is difficult.

Observations of white dwarfs (WDs) provide a promising alternative method to identify XOCs and measure their composition. Between 25 and 50 per cent of WDs exhibit trace amounts of externally derived metals in their atmospheres (Zuckerman et al. 2003, 2010; Barstow et al. 2014; Koester, Gänsicke & Farihi 2014; Wilson et al. 2019). This subset is commonly referred to as polluted WDs. The pollution is generally attributed to continual accretion of debris from a dynamically evolving planetary system (e.g. Debes & Sigurdsson 2002; Debes, Walsh & Stark 2012; Frewen & Hansen 2014; Petrovich & Muñoz 2017; Stephan, Naoz & Zuckerman 2017; Mustill et al. 2018; Maldonado et al. 2020; Li, Mustill & Davies 2022; O'Connor, Teyssandier & Lai 2022; Trierweiler et al. 2022). The cumulative mass and chemical composition of the accreted material provide information about the parent body or bodies (e.g. Zuckerman et al. 2007; Xu et al. 2019; Doyle, Desch & Young 2021; Buchan et al. 2022; Trierweiler, Doyle & Young 2023). Polluted WDs are therefore important probes of extrasolar planetesimal populations.

The characterization of parent bodies producing WD pollution is subtle and subject to uncertainties related to the mixing and settling of metals within the WD's atmosphere. The simplest and most widely implemented methodology accounts only for gravitational settling (Dupuis et al. 1993). The settling time-scale varies significantly along the WD cooling sequence, taking values of $\sim 10^{-2}$–10^{3} yr for a hydrogen-rich atmosphere and $\sim 10^{4}$–10^{6} yr for a helium-rich atmosphere (e.g. Koester 2009; Bauer & Bildsten 2019). Accounting for additional processes such as thermohaline mixing (Deal et al. 2013; Wachlin et al. 2017; Bauer & Bildsten 2018) and convective overshooting (Tremblay et al. 2015, 2017; Bauer & Bildsten 2019; Cunningham et al. 2019) can alter the total metal accretion rate inferred for a given WD. However, these effects do not alter the inferred composition of the accreted material. Radiative levitation can also affect a WD's metal abundances and inferred accretion rate (e.g. Chayer, Fontaine & Wesemael 1995a; Chayer et al. 1995b; Chayer 2014), but only for effective temperatures above 20 000 K.

To date, a few dozen polluted WDs have been the subject of spectroscopic follow-up studies measuring their elemental abundances (Jura & Young 2014; Zuckerman & Young 2018). In general, the accreted material is dominated by the silicate-forming elements O, Mg, Si, and Fe. The measured abundance ratios broadly resemble those found in the CI chondrites (the most pristine meteorites in terms of composition) and the bulk Earth (e.g. Zuckerman et al. 2007; Xu et al. 2019; Doyle et al. 2023; Trierweiler et al. 2023), suggesting that rocky parent bodies are the predominant source of pollution. Debris from an icy parent body such as a comet would also be rich in C and N, producing higher stellar abundances of these volatile elements than are generally observed. For example, Halley's comet is enriched in C and N by $\gtrsim$1 dex by number relative to the CI chondrites (Jessberger, Christoforidis & Kissel 1988; Lodders 2021). At present, the only known polluted WD with C and N abundances comparable to Halley's comet is WD 1425+540 (Xu et al. 2017). This WD is a member of a wide binary system, so gravitational perturbations from the companion star may facilitate the delivery of volatile-enriched icy objects (e.g. Bonsor & Veras 2015; Stephan et al. 2017). Some polluted WDs appear to have accreted water-rich bodies, indicated by the detection of trace hydrogen in helium-dominated atmospheres (e.g. Gentile Fusillo et al. 2017; Hollands, Gänsicke & Koester 2018; Coutu et al. 2019; Hoskin et al. 2020; Izquierdo et al. 2021). Veras, Shannon & Gänsicke (2014) proposed that this can be explained by occasional comet impacts. On the whole, chemical evidence indicates that volatile-enriched exocomets are not the main source of pollution in most WD systems.

In this paper, we address the question of why accretion of volatile-enriched debris is rare among WDs. Alcock, Fristrom & Siegelman (1986) considered this question and argued that the overall fraction of single stars with XOCs is small. However, their conclusion was based on a limited sample of polluted WDs discovered at the time. Moreover, it is now in tension with the apparent ubiquity of volatile-enriched interstellar comets. An alternative explanation is that the dynamical evolution of XOCs around planet-hosting WDs reduces the rate of comet accretion events such that the star's volatile abundances remain below the minimum observable level. For WDs cooler than 20 000 K, the minimum observable accretion rate for rocky debris is a few 10^{5} g s^{-1} (Koester et al. 2014; Blouin & Xu 2022). We assume that the same detection threshold applies to debris from volatile-enriched exocomets.

In this work, we investigate dynamical processes that reduce the rate of comet accretion events for single WDs hosting XOCs. In Section 2, we apply the standard loss cone theory of the delivery of LPCs to estimate the comet accretion rate from a Solar-system-like XOC. In Section 3, we use numerical simulations to study the retention of comets during late stellar evolution. In Section 4, we consider how a surviving planetary system around a WD modifies the rate of comet bombardment. In Section 5, we synthesize the results of the preceding sections, compare our results with those of related works, and provide some qualifications of our conclusions. We also discuss the potential relevance of comets to the question of planetary habitability around WDs. We summarize our main results in Section 6.

2 DYNAMICS OF COMET INJECTION

The dynamical evolution of OC comets is governed by a combination of several effects. These include secular torques due to both the Galactic tidal field and an inner planetary system (Heisler & Tremaine 1986; Section 4.1) and random, impulsive perturbations from stellar flybys (e.g. Oort 1950; Hills 1981; Heisler, Tremaine & Alcock 1987). External perturbations have contributed to the gradual erosion of the OC in the Solar system over its 4.5-Gyr lifetime. Comets with low perihelion distances can be scattered during encounters with planets (e.g. Fernández 1981). These processes lead to either the ejection of comets as free-floating bodies or their capture in the inner Solar system as SPCs. Planets can also tidally disrupt or accrete passing comets, as in Comet Shoemaker–Levy 9's collision with Jupiter (Chapman 1993). Comets passing close to the Sun 'fade' over successive passages (Whipple 1962; Wiegert & Tremaine 1999; Brasser & Wang 2015) or are tidally disrupted.

In the Solar system, the structure of the OC has presumably reached a quasi-steady state after a few Gyr of dynamical relaxation (e.g. Duncan et al. 1987; Higuchi & Kokubo 2015). The progenitors of polluted WDs are generally more massive than the Sun ($\approx$1.5–3 $M_\odot$; Koester et al. 2014) and therefore have shorter main-sequence

lifetimes. A cometary reservoir surrounding a star whose main-sequence lifetime is shorter than the reservoir's relaxation time may differ in structure from the OC. Differences between the architectures of the host's planetary system and the Solar system, as well as the Galactic environments in which the systems formed, can also produce differently structured XOCs (Fernández 1997). Nevertheless, the inferred properties of the OC provide a useful starting point for studying XOCs.

In the following, we use the loss cone theory to determine the injection rate of comets from an XOC (Heisler & Tremaine 1986). First, we introduce the quantities describing the orbits of comets and their distribution within the OC. The mass of the central star is denoted M. We assume that each comet is a mass-less test particle. We denote the usual Keplerian elements as follows: semimajor axis a, eccentricity e, inclination I, argument of periastron χ, longitude of the ascending node Ω, and mean anomaly l. Related quantities are the periastron and apoastron distances $q = a(1 - e)$ and $Q = a(1 + e)$, mean motion $\omega = (GM/a^3)^{1/2}$, and orbital period $P = 2\pi/\omega$. We also refer to the following Delaunay action variables:

$$L = (GMa)^{1/2}, \quad J = L(1 - e^2)^{1/2}, \quad J_z = J\cos I. \tag{1}$$

These are canonically conjugate to l, χ, and Ω, respectively. The action L is related to the orbital energy per unit mass, whilst J and J_z are the magnitude and vertical component of the orbital angular momentum per unit mass. The distribution function f of comets in an XOC specifies the number of comets per volume element of phase space, i.e.

$$\mathrm{d}N = f(L, J, J_z, l, \chi, \Omega)\,\mathrm{d}L\,\mathrm{d}J\,\mathrm{d}J_z\,\mathrm{d}l\,\mathrm{d}\chi\,\mathrm{d}\Omega. \tag{2}$$

In principle, f may also depend explicitly on the time t. We neglect this possibility for simplicity; this is equivalent to assuming the OC is dynamically relaxed.

2.1 Galactic tides

Heisler & Tremaine (1986, hereafter HT86) presented an analytic model of the secular evolution of a star–comet system perturbed by the tidal field of the Galaxy. In their model, the primary star is assumed to follow a circular orbit in the Galactic mid-plane. The Galactic potential $\Phi_{\rm GT}$ near the star can be approximated as the potential inside a slab with uniform density $\rho_{\rm g}$, i.e.

$$\Phi_{\rm GT} = 2\pi G\rho_{\rm g} z^2, \tag{3}$$

where z is the vertical distance from the Galactic mid-plane. We adopt a fiducial value $\rho_{\rm g} = 0.1\,\mathrm{M}_\odot\,\mathrm{pc}^{-3}$ throughout this work (e.g. McKee, Parravano & Hollenbach 2015). HT86 considered the secular evolution of the comet, obtained by averaging $\Phi_{\rm GT}$ over the Keplerian orbit before applying Hamilton's equations. For the purposes of this paper, we require only the equations of motion for J and χ:

$$\frac{\mathrm{d}J}{\mathrm{d}t} = -\frac{5}{2}\omega_{\rm GT} L\left(1 - \frac{J^2}{L^2}\right)\left(1 - \frac{J_z^2}{J^2}\right)\sin(2\chi), \tag{4a}$$

$$\frac{\mathrm{d}\chi}{\mathrm{d}t} = \omega_{\rm GT}\frac{J}{L}\left[1 - 5\left(1 - \frac{J_z^2 L^2}{J^4}\right)\sin^2\chi\right]. \tag{4b}$$

In equation (4), the characteristic oscillation frequency $\omega_{\rm GT}$ is given by

$$\omega_{\rm GT} = G\rho_{\rm g} P \approx \frac{1}{2.2\,\mathrm{Gyr}}\left(\frac{\rho_{\rm g}}{0.1\,\mathrm{M}_\odot\,\mathrm{pc}^{-3}}\right)\left(\frac{a}{10^4\,\mathrm{au}}\right)^{3/2}\left(\frac{M}{\mathrm{M}_\odot}\right)^{-1/2}. \tag{5}$$

2.1.1 Comet injection rate at small distances

HT86 calculated the rate at which comets are injected by the Galactic tide within a critical distance $q_{\rm cr} \ll a$ of the central star from a spherically symmetric cloud with distribution function $f(L, J)$. Their purpose was to estimate the rate at which OC comets are captured within the inner Solar system via encounters with the planets. In the absence of gravitational perturbations from a planetary system, we may use their result to estimate the flux of OC comets at arbitrarily small distances.

It is convenient to denote the orbital angular momentum of an object with perihelion distance $q_{\rm cr}$ as

$$J_{\rm cr} \equiv (2GMq_{\rm cr})^{1/2} \tag{6}$$

with $J_{\rm cr} \ll L$. For a given $J_{\rm cr}$, we denote the injection rate of comets between L and $L + \mathrm{d}L$ as $\Gamma(L)\,\mathrm{d}L$ and the total rate as

$$\Gamma_{\rm tot} = \int_0^\infty \Gamma(L)\,\mathrm{d}L. \tag{7}$$

The phase-space region $J \le J_{\rm cr}$ is called the 'loss cone' (or 'loss cylinder') because comets passing through this region are assumed to be removed from the XOC.

There are two regimes of the comet injection process, called the 'empty loss cone' and 'filled loss cone'. These correspond to different expressions for $\Gamma(L)$, in particular, ranges of L. The loss cone is said to be empty when $\Delta J \lesssim J_{\rm cr}$, where $\Delta J \sim |\dot{J}|P$ is the typical change of J per orbit. The injection rate for an empty loss cone is (HT86)

$$\Gamma_{\rm e}(L)\,\mathrm{d}L \simeq \frac{160\pi^3\rho_{\rm g}L^4 J_{\rm cr}}{3GM^2} f(L, J_{\rm cr})\,\mathrm{d}L, \tag{8}$$

where $J_{\rm cr} \ll L$. This is calculated as the rate at which comets with $J \in [J_{\rm cr}, J_{\rm cr} + \mathrm{d}J)$ are pushed by the Galactic tide across the boundary of the loss cone. The loss cone is filled when $\Delta J \gtrsim J_{\rm cr}$; the corresponding injection rate at a given L is (HT86)

$$\Gamma_{\rm f}(L)\,\mathrm{d}L \simeq \frac{4\pi^2(GM)^2 J_{\rm cr}^2}{L^3} f(L, J_{\rm cr})\,\mathrm{d}L. \tag{9}$$

This is equal to the steady-state number of comets inside the loss cone ($J \le J_{\rm cr}$) divided by their orbital period $P(L)$. Because $\Delta J \propto L^7 \propto a^{7/2}$, the loss cone is empty (filled) for small (large) L or a. The transition occurs when $\Delta J \simeq J_{\rm cr}$ or, equivalently, the two expressions for $\Gamma(L)$ are equal:

$$a_{\rm eq} = 0.38\left(\frac{M^2 q_{\rm cr}}{\rho_{\rm g}^2}\right)^{1/7} \approx 2.6\times10^4\,\mathrm{au}\left(\frac{M}{\mathrm{M}_\odot}\frac{0.1\,\mathrm{M}_\odot\,\mathrm{pc}^{-3}}{\rho_{\rm g}}\right)^{2/7}\left(\frac{q_{\rm cr}}{1\,\mathrm{au}}\right)^{1/7}. \tag{10}$$

Fig. 1 depicts the differences between the empty and filled loss cone regimes schematically.

We estimate the injection rate as a function of L as

$$\Gamma(L) = \begin{cases}\Gamma_{\rm e}(L), & L < L_{\rm eq};\\ \Gamma_{\rm f}(L), & L \ge L_{\rm eq},\end{cases} \tag{11}$$

where $L_{\rm eq} = (GMa_{\rm eq})^{1/2}$. We then have

$$\Gamma_{\rm tot} = \int_{L_1}^{L_{\rm eq}} \Gamma_{\rm e}(L)\,\mathrm{d}L + \int_{L_{\rm eq}}^{L_2} \Gamma_{\rm f}(L)\,\mathrm{d}L, \tag{12}$$

where $L_{1,2} = (GMa_{1,2})^{1/2}$ correspond to the inner and outer edges of the XOC. For most realistic distribution functions, $\Gamma(L)$ has a peak

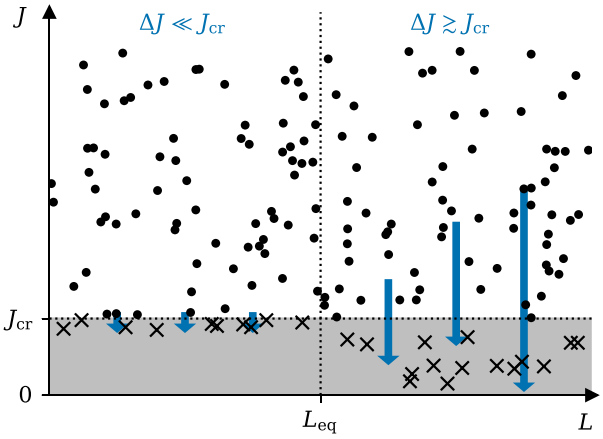

Figure 1. Schematic depiction of the loss cone theory of comet injection. Blue arrows represent the typical change of a comet's angular momentum per orbit (ΔJ). For $\Delta J \ll J_{\rm cr}$ ($L \lesssim L_{\rm eq}$), XOC comets (dark points) are injected by diffusing slowly across the boundary of the cone ($J = J_{\rm cr}$); the interior of the loss cone (shaded region) is empty because the comets are lost within one orbital period (crosses). For $\Delta J \gtrsim J_{\rm cr}$ ($L \gtrsim L_{\rm eq}$), comets leap over the boundary and fill the loss cone before being lost.

around $L = L_{\rm eq}$; thus,

$$\Gamma_{\rm tot} \sim L_{\rm eq}\, \Gamma(L_{\rm eq}) \propto \frac{M^2 q_{\rm cr}}{a_{\rm eq}} f(L_{\rm eq}, J_{\rm cr}). \tag{13}$$

We set $a_2 = 10^5$ au unless otherwise specified. We investigate the effect of varying a_1 below.

2.1.2 Fiducial distribution function

In order to evaluate $\Gamma_{\rm tot}$, we must specify the distribution function $f(L, J)$. Let the number density profile of comets in the XOC be $n(a)$, and let the eccentricity distribution be $f_{\rm e}(e)$. We assume that $f_{\rm e}$ is independent of semimajor axis. We then have

$$\begin{aligned} {\rm d}N &= f(L,J)\,{\rm d}L\,{\rm d}J \int_{-J}^{J} {\rm d}J_z \int_0^{2\pi} {\rm d}l \int_0^{2\pi} {\rm d}\chi \int_0^{2\pi} {\rm d}\Omega \\ &= (2\pi)^3 2J f(L,J)\,{\rm d}L\,{\rm d}J \\ &\equiv 4\pi a^2 n(a) f_e(e)\,{\rm d}a\,{\rm d}e, \end{aligned} \tag{14}$$

relating $n(a)$ and $f_{\rm e}(e)$ to $f(L, J)$. In the following, we assume that comets have a 'thermal' eccentricity distribution $fe(e) = 2e$ (Jeans 1919; Ambartsumian 1937); in this case, f is independent of J.

Simulations of OC formation and evolution (e.g. Duncan et al. 1987; Leto et al. 2008; Higuchi & Kokubo 2015) generally predict a centrally concentrated density profile, often approximated as a truncated power law:

$$n(a) \propto a^{-\alpha} \qquad (a_1 \le a \le a_2). \tag{15}$$

We adopt this as our fiducial density profile. Thus, our fiducial distribution function is

$$f(L,J) = \begin{cases} C N_{\rm c} (L/L_1)^{3-2\alpha}, & L_1 \le L \le L_2; \\ 0, & \text{else.} \end{cases} \tag{16}$$

The normalization constant is

$$C = \begin{cases} (\alpha-3)\left[4\pi L_1^3 \left(1-(L_1/L_2)^{2\alpha-6}\right)\right]^{-1}, & \alpha \neq 3; \\ \left[8\pi^3 L_1^3 \ln(L_2/L_1)\right]^{-1}, & \alpha = 3. \end{cases} \tag{17}$$

The value of α is typically taken to be between 2 and 4.

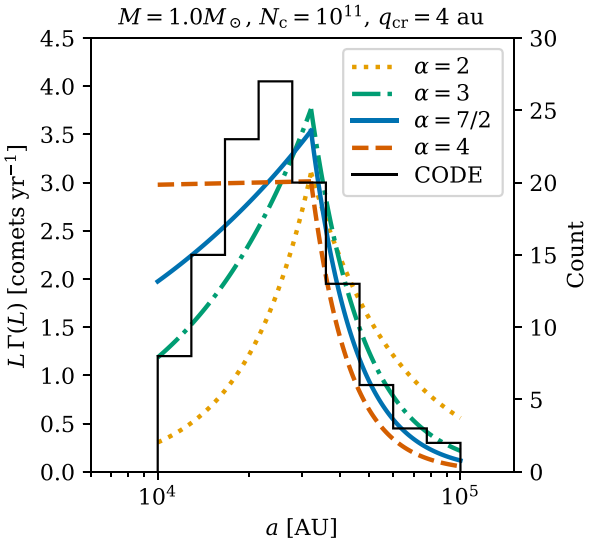

Figure 2. Predicted incremental distribution of dynamically new comets with respect to a for four fiducial OC models (coloured curves), as predicted by the HT86 formalism. All models contain the same number of comets but have different density exponents α. The black histogram shows the distribution of 117 observed comets with $a \ge 10^4$ au and $q \le 4$ au in CODE (Królikowska & Dybczyński 2020).

2.1.3 LPC flux in the solar system

In this section, we illustrate the validity and limitations of the formalism derived by HT86. We apply it to estimate the flux of 'dynamically new' LPCs (defined as those with $a \ge 10^4$ au) into the inner Solar system and their incremental distribution with respect to a. These are given by the quantities $\Gamma_{\rm tot}$ and $L\,\Gamma(L)$. We set $q_{\rm cr} = 4$ au (and thus $J_{\rm cr} = [2G\,{\rm M}_\odot q_{\rm cr}]^{1/2}$) in this exercise, corresponding to $a_{\rm eq} = 3.2 \times 10^4$ au.

We adopt a fiducial OC model containing $N_{\rm c} = 10^{11}$ comets distributed spherically between $a_1 = 10^4$ au and $a_2 = 10^5$ au with a power-law exponent in equation (15) of $\alpha = 7/2$. This is motivated by theoretical OC formation models (Duncan et al. 1987; Vokrouhlický et al. 2019). The predicted total flux is $\Gamma_{\rm tot} = 2.1\,{\rm yr}^{-1}$, with $1.6\,{\rm yr}^{-1}$ coming from the empty loss cone ($a < a_{\rm eq}$) and $0.5\,{\rm yr}^{-1}$ from the filled loss cone ($a > a_{\rm eq}$). This lies at the lower end of the range of observational estimates $\sim$1–10 yr^{-1} (e.g. Everhart 1967; Whipple 1978; Hughes 2001; Francis 2005; Bauer et al. 2017; Boe et al. 2019). Fig. 2 shows the distribution of new LPCs predicted by the HT86 formalism for this model as a solid blue curve. To assess the accuracy of the predicted LPC distribution, we compare it with a sample of 117 comets with $a \ge 10^4$ au and $q \le 4$ au from the Catalogue of Cometary Orbits and their Dynamical Evolution (CODE; Królikowska & Dybczyński 2020). The model reproduces the observed distribution moderately well. The 'Oort peak' of observed comets at $a \approx 2.5 \times 10^4$ au roughly matches the predicted location ($a = a_{\rm eq} \approx 3.2 \times 10^4$ au), although the number of comets with $a \lesssim 2 \times 10^4$ au decreases more steeply than the model predicts.

We also show in Fig. 2 the predicted LPC distributions for several other OC models with the same $N_{\rm c}$ and $a_{1,2}$ but different α. The predicted total fluxes ($\approx$1–2 yr^{-1}) are roughly equal for all α, but the incremental distributions vary significantly. The relative number of comets with $a < 2 \times 10^4$ au is somewhat sensitive to α. The models with $\alpha = 2$ and 4 are poor matches to the observed distribution, but $\alpha = 3$ matches about as well as the $\alpha = 7/2$ model. As evident from Fig. 2, a single-power-law model of the OC cannot perfectly

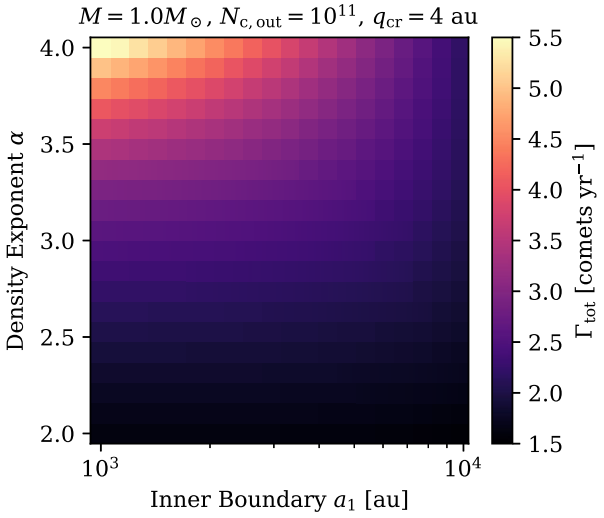

Figure 3. Heat map showing the total LPC flux in OC models with a spherical inner extension ('Hills cloud') as a function of the density power-law exponent α and inner boundary distance a_1. The number of comets with $a > 10^4$ au is held fixed.

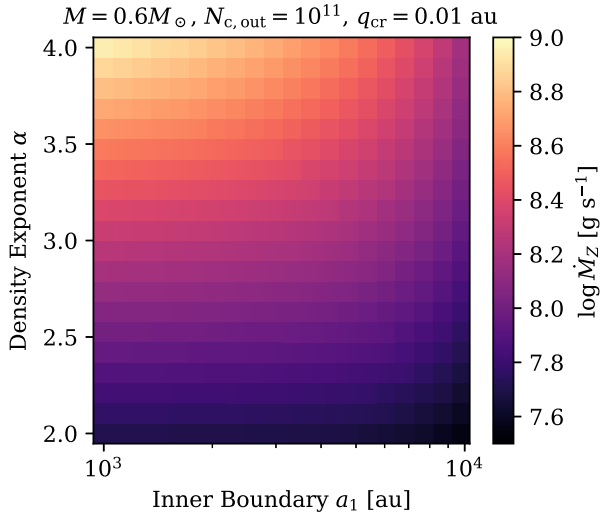

Figure 4. Similar to Fig. 3, this heat map shows the expected metal accretion rate (as log $\dot{M}_Z$) of a 0.6-$M_\odot$ WD from XOC comets as a function of α and a_1. Each accretion event is assumed to contribute a mass $f_{acc} m_c = 10^{17}$ g of metals to the atmosphere.

reproduce the observed distribution of dynamically new comets. However, models with $\alpha \approx 3$–3.5 are adequate to reproduce the broad features. For the remainder of this work, we adopt $\alpha = 7/2$ unless otherwise specified.

The 'inner' OC ($a < 10^4$ au, also known as the Hills cloud) was not considered an important source of LPCs until relatively recently (e.g. Kaib & Quinn 2009; Dybczyński & Królikowska 2011). Comet orbits, in this region, are dynamically stabler because the Galactic tide is weaker ($\dot{J} \propto a^2$, equation 4a). The Jovian planets affect inner OC comets more strongly as they approach the inner Solar system, sometimes making them appear to originate from the outer OC (Kaib & Quinn 2009). Meanwhile, theoretical studies of OC formation and evolution have predicted a variety of cloud populations and density profiles interior to 10^4 au (e.g. Duncan et al. 1987; Kaib & Quinn 2008; Vokrouhlický et al. 2019). The properties of the inner OC are therefore highly uncertain, but potentially significant.

Faced with these uncertainties, it is instructive to see how the predicted LPC flux changes when we include a spherically symmetric, dynamically relaxed inner OC in our model. We therefore repeat the previous exercise for a variety of OC models in which the density profile is extended inward to an inner boundary distance a_1, keeping the number of comets with $a > 10^4$ au constant. We show the predicted comet flux Γ_{tot} in Fig. 3 for a grid of a_1 and α values. The value of Γ_{tot} is more sensitive to a_1 for larger α, i.e. for more centrally concentrated density profiles. The LPC flux varies by a factor of $\approx$4 over this section of parameter space, never exceeding $\approx 6\,\mathrm{yr}^{-1}$. Thus, the presence of an inner OC increases the potential LPC flux only by a factor of a few.

Overall, the HT86 formalism, coupled to a spherical, dynamically relaxed OC model with a power-law density profile, provides a good estimate of the LPC flux in the Solar system, although some properties of the OC are relatively unconstrained. The formalism also broadly reproduces the observed distribution of semimajor axes.

2.1.4 WD pollution from XOC comets

In this section, we estimate the metal accretion rate of a WD due to the tidal disruption of LPCs with small periastron distances. We apply analogous calculations as in the previous subsection, assuming a typical WD with mass $M \approx 0.6\,M_\odot$. We assume that the comets are rubble piles with uniform mass density ρ_c and zero internal strength. Therefore, the comets are tidally disrupted when they pass closer within a distance r_{tide} of the WD, where

$$r_{tide} \simeq \left(\frac{M}{\rho_c}\right)^{1/3} \approx 8 \times 10^{-3}\,\mathrm{au} \left(\frac{M}{0.6\,M_\odot}\right)^{1/3} \left(\frac{\rho_c}{0.6\,\mathrm{g\,cm^{-3}}}\right)^{-1/3}. \quad (18)$$

For simplicity, we assume that there are no planets orbiting the WD massive enough to perturb the orbits of LPCs. Although comets pass close to the WD, short-range dynamical effects such as general relativistic precession have a negligible effect on the rate at which comets enter the loss cone. This is because the Galactic tidal torque is applied mainly near apoastron. The HT86 formalism can therefore be used to estimate the tidal disruption rate Γ_{dis}. This disruption rate is equal to the value of Γ_{tot} when $q_{cr} = r_{tide}$ ($J_{cr} = [2GMr_{tide}]^{1/2} \equiv J_{tide}$). The disruption rate is related, in turn, to the rate $\dot{M}_Z$ at which metal-rich debris pollutes the WD atmosphere. If the average mass of a comet is m_c and a fraction f_{acc} of the debris from each comet is eventually accreted by the WD, then

$$\dot{M}_Z = f_{acc} m_c \Gamma_{dis}. \quad (19)$$

We adopt a representative value $m_c = 10^{17}$ g, corresponding to a total OC mass $M_{OC} = m_c N_c = 1.7 M_\oplus (N_c/10^{11})$ (cf. Weissman 1996; Francis 2005; Boe et al. 2019). For a spherical body of density $\rho_c = 0.6\,\mathrm{g\,cm^{-3}}$, $m_c = 10^{17}$ g corresponds to a radius of 3.4 km.

We assume that single WDs have XOCs with broadly similar properties to the OC in the Solar system. Adopting a representative value $q_{cr} = r_{tide} \approx 0.01$ au, we find $a_{eq} = 1.2 \times 10^4$ au. It is straightfoward to calculate $\dot{M}_Z$ for the family of models from the previous section. Fig. 4 shows the result in an analogous manner to Fig. 3. We find

$$\dot{M}_Z \sim 10^{8\pm1}\,\mathrm{g\,s^{-1}} \left(\frac{f_{acc} m_c}{10^{17}\,\mathrm{g}}\right) \left(\frac{N_{c,out}}{10^{11}}\right), \quad (20)$$

where $N_{c,out}$ is the number of comets with $a > 10^4$ au. Note that the magnitude of $\dot{M}_Z$ is much more sensitive to a_1 and α in this case

because of the smaller value of $q_{\rm cr}$ (and hence $a_{\rm eq}$). This shows the importance of accounting for the possible existence of an inner OC around a WD, even if this region does not necessarily dominate the LPC flux in the Solar system.

2.2 Stellar flybys

2.2.1 Weak encounters

Distant stellar flybys induce weak stochastic perturbations on OC comets, leading to diffusion of individual comets in phase space. This diffusion replenishes the supply of comets near the edge of the loss cone, which is why Galactic tides are able to inject comets continually on Gyr time-scales. Flybys can also inject comets directly into the loss cone, increasing the accretion rate over that due to Galactic tides alone.

As a first approximation, we may direct comet injection by flybys as an independent process from injection by the Galactic tide (but see Collins & Sari 2010 for an example of treating them simultaneously). Under this assumption, HT86 showed the comet injection rate due to weak flybys has a similar behaviour to the rate due to the Galactic tide. As before, there are distinct regimes where the loss cone is empty and filled. The transition distance between regimes is modified by the fact that only stars contribute to the density (cf. equation 10):

$$a_{\rm eq*} = 0.32 \left(\frac{M^2 q_{\rm cr}}{\rho_*^2} \right)^{1/7}, \tag{21}$$

where ρ_* is the mean stellar density of the Galactic environment. The differential and total injection rates due to stellar flybys, $\Gamma_*(L)$ and $\Gamma_{\rm tot*}$, have the same essential scalings as in the tidal problem. By equation (13), the ratio of the comet injection rates from each mechanism is

$$\frac{\Gamma_{\rm tot*}}{\Gamma_{\rm tot}} \sim \frac{a_{\rm eq}}{a_{\rm eq*}} \frac{f(L_{\rm eq*}, J_{\rm cr})}{f(L_{\rm eq}, J_{\rm cr})} = \left(\frac{\rho_*}{\rho_{\rm g}} \right)^{(2\alpha-1)/7}. \tag{22}$$

The stellar mass density of the Galactic disc, ρ_*, is somewhat less than $\rho_{\rm g}$; for example, in the solar neighbourhood, $\rho_* = 0.04\,{\rm M}_\odot\,{\rm pc}^{-3}$ versus $\rho_{\rm g} = 0.1\,{\rm M}_\odot\,{\rm pc}^{-3}$ (e.g. Flynn et al. 2006; McKee et al. 2015). Therefore, we expect $\Gamma_{\rm tot*}/\Gamma_{\rm tot} \lesssim 1$ for a realistic α. HT86 argued on this basis that Galactic tides are the dominant mechanism by which LPCs are injected into the inner Solar system (except during comet showers; see below). The same reasoning applies to comets orbiting WDs in the Galactic disc. The metal accretion rate derived from Galactic tides and weak stellar flybys together is therefore predicted to be approximately the same as that due to tides alone.

In reality, Galactic tides and stellar flybys are not separable processes. Rickman et al. (2008) and Fouchard et al. (2011a,b) performed numerical simulations including tides and flybys operating either simultaneously or independently. They found that the total injection rate when both processes operate simultaneously is a factor of few larger than the sum of the rates from each process acting independently. Additionally, Torres et al. (2019) showed that the relative importance of tides and flybys is sensitive to the radial extent of the OC. Specifically, tides are relatively more important for extensive clouds, while flybys are more important for compact clouds. We discuss these complications further in Section 5.3.1.

2.2.2 Comet showers

Field stars occasionally pass through the inner portion of the OC, triggering comet showers. During these events, the comet injection rate is enhanced by at least an order of magnitude (Hills 1981; Heisler et al. 1987). If XOCs are common around WDs, then comet showers could elevate the rate of metal accretion over the 'background' rate due to Galactic tides and weak flybys.

Comet showers are relatively infrequent events. The duration $\Delta t_{\rm close} = b/v_*$ of a close encounter with a field star with impact parameter b and speed v_* is short compared to the orbital period of a comet at the same distance. Therefore, the duration of each shower is of the order of P. For a typical v_*, we use the 3D velocity dispersion of thin-disc stars from Anguiano et al. (2020). This gives

$$\Delta t_{\rm close} \approx 10^{-3}\,{\rm Myr} \left(\frac{b}{10^4\,{\rm au}} \right) \left(\frac{v_*}{50\,{\rm km\,s^{-1}}} \right)^{-1}, \tag{23}$$

$$P \approx 1.3\,{\rm Myr} \left(\frac{b}{10^4\,{\rm au}} \right)^{3/2} \left(\frac{M}{0.6\,{\rm M}_\odot} \right)^{-1/2}. \tag{24}$$

Meanwhile, the expected interval between flybys with impact parameter closer than a distance b is

$$\Delta t_{\rm flyby} = \frac{1}{\pi b^2 n_* v_*} \approx 30\,{\rm Myr} \left(\frac{b}{10^4\,{\rm au}} \right)^{-2} \left(\frac{n_*}{0.1\,{\rm pc^{-3}}} \right)^{-1} \left(\frac{v_*}{50\,{\rm km\,s^{-1}}} \right)^{-1}, \tag{25}$$

where n_* is the number density of field stars. In practice, only stars more massive than the WD can trigger comet showers (Heisler et al. 1987). This effectively reduces n_* from the nominal value by a factor related to the stellar mass function, for the purposes of determining the frequency of comet showers. Using a nominal WD mass $M = 0.6\,{\rm M}_\odot$, and assuming that passing stars are drawn from the present-day mass function fitted by Bovy (2017), we estimate the fraction of close flybys by stars more massive than M to be $f_M \approx 0.14$. If comet showers occur for $b \leq 10^4$ au, then their 'duty cycle' is

$$p_{\rm sh} = \frac{f_M P}{\Delta t_{\rm flyby}} \approx 6 \times 10^{-3} \left(\frac{b}{10^4\,{\rm au}} \right)^{7/2} \left(\frac{f_M n_*}{0.014\,{\rm pc^{-3}}} \frac{v_*}{50\,{\rm km\,s^{-1}}} \right). \tag{26}$$

A comet-hosting WD therefore has an $\sim$1 per cent probability of being in the midst of a comet shower when we observe it. In a sample of $\mathcal{N}$ single WDs that possess XOCs, the probability that a comet shower is ongoing in one system is

$$\mathcal{N} p_{\rm sh} (1 - p_{\rm sh})^{\mathcal{N}-1}. \tag{27}$$

Detailed spectroscopic analyses that constrain the presence of volatiles have been published for a few dozen WDs at present (e.g. Koester et al. 2014). For a nominal value $p_{\rm sh} = 0.006$, we calculate a $\approx$15 per cent probability of an ongoing comet shower in a sample of size $\mathcal{N} = 30$. Thus, the current subset of polluted WDs with constrained volatile abundances may not be large enough to constrain the occurrence of comet showers.

2.3 Synthesis

Our model predicts that, if single WDs possess XOCs with properties broadly similar to the Solar system's OC, a large fraction would be polluted by volatile-rich debris with characteristic accretion rates $\dot{M}_Z \sim 10^{8\pm1}\,{\rm g\,s^{-1}}$ (see equation 20). The predicted $\dot{M}_Z$ is consistent with the median inferred accretion rate among polluted WDs, which is around $10^8\,{\rm g\,s^{-1}}$ (e.g. Wyatt et al. 2014; Xu et al. 2019; Blouin & Xu 2022). The minimum accretion rate required for pollution to be detected in a typical WD atmosphere is $\sim 10^5\,{\rm g\,s^{-1}}$ (e.g. Koester et al. 2014; Blouin & Xu 2022). The predicted pollution would therefore

be detectable by current observations, even if the accretion process is fairly inefficient ($f_{\rm acc} \sim 0.01$–0.1). It is difficult to explain the paucity of polluted WD atmospheres with a comet-like composition within the standard theory of comet delivery from an XOC.

There are three main possibilities to explain this apparent discrepancy:

(i) XOCs are intrinsically rare around WD progenitors.
(ii) XOCs are depleted during late stellar evolution.
(iii) Additional dynamical processes interfere with the delivery of XOC comets to extremely small periastron distances ($q \sim r_{\rm tide}$).

Option (i) has not been ruled out by direct observations. However, it would be difficult to reconcile this scenario with the longstanding idea that XOC formation is an expected byproduct of the formation and early dynamical evolution of giant planets (e.g. Duncan et al. 1987; Hahn & Malhotra 1999; Vokrouhlický et al. 2019). The progenitors of polluted WDs are more massive than the Sun on average (e.g. Koester et al. 2014), and the occurrence rate of giant planets has a positive correlation with stellar mass (e.g. Johnson et al. 2010; Reffert et al. 2015; Jones et al. 2016; Ghezzi, Montet & Johnson 2018). If indeed giant-planet formation typically results in XOC formation, then WD progenitors may be more likely to possess XOCs than solar-mass stars. The Galactic population of interstellar interlopers may also be consistent with ubiquitous XOC formation (Do et al. 2018; but see Moro-Martín 2018, 2019). In the next two sections, therefore, we consider two mechanisms that could plausibly contribute to options (ii) and (iii).

3 STELLAR MASS-LOSS

The effects of stellar evolution on OC comets are most pronounced during the asymptotic giant branch (AGB) phase, when the star ejects a large fraction of its mass in a wind. Mass-loss causes cometary orbits to expand and possibly become unbound (Veras et al. 2011). If AGB mass-loss is somewhat asymmetric, a natal kick is imparted to the WD. The typical time-scale of AGB mass-loss ($\sim$0.1–1 Myr) and WD kick speed ($\sim$1 km s^{-1}; e.g. Heyl 2007, 2008a, b; Davis et al. 2008; Heyl & Penrice 2009; Fregeau et al. 2009; Izzard, Dermine & Church 2010; El-Badry & Rix 2018) are comparable to the orbital period and velocity of OC objects. These effects will reduce the number of comets in the cloud and may alter their orbital distribution function. In this section, we evaluate to what extent these processes reduce the WD comet accretion rate. In Section 3.1, we describe our parametric model for stellar mass-loss. In Section 3.2, we conduct a series of numerical integrations of XOC objects in the context of this model. Previous studies along similar lines include Parriott & Alcock (1998), Veras et al. (2014), Stone, Metzger & Loeb (2015), and Caiazzo & Heyl (2017). We compare our methods and results to theirs in Section 5.1.

3.1 Asymmetric mass-loss

Consider a star with mass M steadily ejecting material at a rate $\dot{M}$. We assume that the outflow exhibits a moderate asymmetry, such that the star receives a recoil acceleration in a fixed direction (unit vector $\hat{\boldsymbol{k}}$). This acceleration is given by

$$\boldsymbol{g}_* = \frac{u_{\rm e}\dot{M}}{M}\hat{\boldsymbol{k}}, \tag{28}$$

where $u_{\rm e}$ is an effective 'exhaust speed' determined by the velocity and geometry of the outflow. The final velocity of the star with respect to its initial rest frame is

$$\boldsymbol{V}_{\rm k} = u_{\rm e} \ln\left(\frac{M_{\rm i}}{M_{\rm f}}\right)\hat{\boldsymbol{k}}\,. \tag{29}$$

In equation (29), $M_{\rm i}$ and $M_{\rm f}$ are the initial and final mass of the star, respectively, which are given roughly by the zero-age main sequence mass ($M_{\rm i} \equiv M_{\rm ms}$) and the WD mass ($M_{\rm f} \equiv M_{\rm wd}$). We adopt fiducial values $M_{\rm ms} = 2.0\,{\rm M}_\odot$ and $M_{\rm wd} = 0.56\,{\rm M}_\odot$ based on the theoretical initial–final mass relation of Choi et al. (2016).

We assume that the stellar mass decreases exponentially after $t = 0$ according to

$$M(t) = M_{\rm ms}\left(\frac{M_{\rm ms}}{M_{\rm wd}}\right)^{-t/T}, \tag{30}$$

until it reaches the final mass $M_{\rm wd}$ at $t = T$. This model has the helpful property that $M/\dot{M}$ is constant, meaning that g_* is constant as well.

This parametric mass-loss model is admittedly idealized. In detailed evolutionary models, late-stage mass-loss takes place in 'bursts' coinciding with thermal pulses on the AGB. To complicate the situation further, the recoil acceleration may not have a fixed direction throughout mass-loss. This symmetry breaking could change the resulting dynamics of injected comets.

3.2 Numerical setup

We perform simulations of comets orbiting a star undergoing continuous mass-loss with REBOUND (Rein & Liu 2012). The Newtonian equations of motion are solved in the rest frame of the central star. We include the effects of stellar mass-loss via the `modify_mass` operator in the extension package REBOUNDX (Kostov et al. 2016; Tamayo et al. 2020). This operator causes the mass of a particle – in this case the central star – to grow or decay exponentially on a user-defined time-scale as described above. Mass-loss in REBOUNDX is assumed to be isotropic. To simulate the effects of asymmetric mass-loss, we include an additional fictitious force per unit mass acting on the comet, defined to be equal and opposite to the recoil acceleration of the central star with respect to an inertial frame.

The goals of our simulations are as follows:

(i) To evaluate the fraction of OC comets that remain bound to a star after AGB mass-loss and a kick.
(ii) To examine the change of the distribution function of comets as a result of these processes.
(iii) To test how varying the mass-loss time-scale and the magnitude of the kick imparted to the star affects these outcomes.

3.2.1 *Initial conditions and parameters*

We initialize all of our simulations with a 2.0-M$_\odot$ star at rest at the origin and a single comet in orbit. We generate the astrocentric orbital elements of each comet as follows: The semimajor axis is drawn from a power-law radial density profile with $\alpha = 7/2$ between 10^3 and 10^5 au, and the other elements are drawn from their respective isotropic distributions (uniform in e^2, $\cos I$, χ, Ω, and l). Note that we define the inclination I relative to the axis of the WD kick in this discussion.

The time-scale of mass-loss and the magnitude of the recoil acceleration are chosen such that, over the duration T of each simulation, the central star evolves to a final mass of 0.56 M$_\odot$ and attains a given speed $V_{\rm k}$ with respect to its original rest frame. We

conduct simulations using the following values of these parameters:

$$T = \{1 \times 10^4, 3 \times 10^4, 1 \times 10^5\}\,\mathrm{yr},$$
$$V_\mathrm{k} = \{0, 0.125, 0.25, 0.50, 0.75, 1.00, 1.25, 1.50\}\,\mathrm{km\,s^{-1}}.$$

These values of T are representative of the range of time-scales on which WD kicks are thought to be imparted. However, these time-scales are somewhat shorter than the overall duration of AGB mass-loss. We therefore tend to overestimate the magnitude of mass-loss-related effects on an XOC. The values of V_k are based on the dispersion of WD kick speeds inferred by El-Badry & Rix (2018) from the occurrence rates of wide binaries containing WDs observed by *Gaia*.

3.2.2 Procedure and post-processing

For each combination (T, V_k), we conduct 10^4 single-comet integrations in REBOUND. We use the IAS15 integrator (Rein & Spiegel 2015) with a sufficiently small time-step to resolve the periastron passage of each comet.

At the end of each integration, we compute the new Keplerian orbit of each comet. The fate of each comet – either ejection or retention – is prescribed as follows. We consider a comet ejected if (a) its final orbit is open ($e \geq 1$) or (b) its final orbit is closed ($e < 1$) but has an apoastron distance $Q = a(1 + e)$ greater than the Hill radius of a WD in the solar neighbourhood (about 0.8 pc). Comets meeting condition (b) are bound to the newborn WD in the context of the two-body problem but in practice are likely to be stripped by the Galactic tide or field stars. Comets that do not satisfy (a) or (b) are considered to be retained by the WD.

A fraction of the 'ejected' comets are on incoming orbits with small q. These comets may experience one final close approach to the WD before ejection. It is possible that some of these objects are tidally disrupted and accreted by the newborn WD (see Stone et al. 2015). However, these comets will still be ejected within an orbital period; they are not relevant for the long-term pollution of the WD.

3.3 Numerical results

3.3.1 Retention of OC comets

Fig. 5 shows the fraction of comets retained in our simulations, f_ret. This fraction decreases steadily with increasing kick speed, since the chosen non-zero values of V_k are comparable to, or larger than, the escape speed near the inner edge of the cloud. For a fixed V_k, f_ret changes by less than a factor of 2 for different T, at least for the range of values we tested.

To gauge the range of likely values for f_ret in real systems, we consider a Maxwellian distribution for the WD kick speeds with dispersion $\sigma = 0.5\,\mathrm{km\,s^{-1}}$, with a probability density function

$$f_V(V_\mathrm{k}) = \sqrt{\frac{2}{\pi}}\frac{V_\mathrm{k}^2}{\sigma^3}\exp\left(-\frac{V_\mathrm{k}^2}{2\sigma^2}\right). \tag{31}$$

The same distribution was used by El-Badry & Rix (2018) to explain the separation distribution of wide binaries containing WDs. We show this distribution in the upper panel of Fig. 5. The mode of the distribution is $V_\mathrm{k} = \sqrt{2}\sigma \approx 0.7\,\mathrm{km\,s^{-1}}$, which gives a retention fraction of ≈0.1. About 90 per cent of newborn WDs would retain a fraction $0.03 \leq f_\mathrm{ret} \leq 0.3$ of their OC comets. This suggests that the rate of WD comet accretion due to Galactic tides would be reduced compared to the estimate in Section 2.1.4 by a factor of ∼3–30 with all else equal. However, we have not yet taken into account the change of the distribution function of the surviving comets.

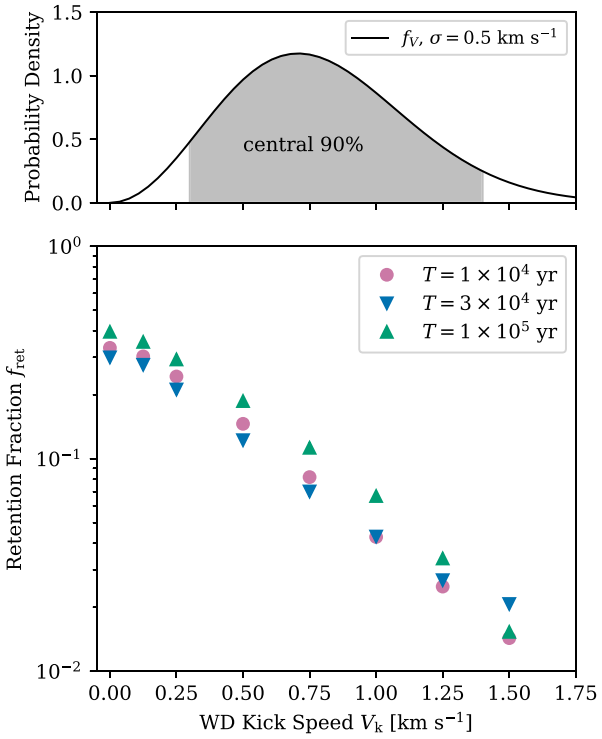

Figure 5. Lower panel: fraction of comets retained in bound orbits as a function of the kick speed V_k imparted to the WD (horizontal axis) and the stellar mass-loss time-scale (different shapes and colours). Each point represents an ensemble of 10^4 simulations. Upper panel: The black curve shows a Maxwellian distribution of kick speeds (equation 31) with $\sigma_\mathrm{k} = 0.5\,\mathrm{km\,s^{-1}}$. The shaded region indicates the central 90 per cent quantile range.

3.3.2 Distribution function of retained comets

In order to use the formalism of HT86 to estimate the rate of comet injection after stellar evolution, we need to characterize the distribution function $f(L, J, \cdots)$ of surviving comets near the edge of the loss cone ($J \ll L$). By construction, the distribution function of surviving comets is uniform with respect to Ω if this angle is measured in the plane normal to the recoil acceleration. The surviving comets will exhibit a highly non-uniform distribution with respect to l because comets near periastron ($l \approx 0, 2\pi$) during late stellar evolution are preferentially retained. However, this distribution will be isotropized over many orbits. We therefore proceed assuming a uniform distribution of l when calculating the injection rate. For convenience, we define a modified apsidal angle

$$\tilde{\chi} \equiv 2\chi \mod 2\pi, \tag{32}$$

so that comets that are pushed inward by the Galactic tide ($\dot{J} < 0$) have $0 < \tilde{\chi} < \pi$ (see equation 4b).

In Fig. 6, we show the distribution of the surviving comets in the planes (a_fin, e_fin^2), (a_fin, $\cos I_\mathrm{fin}$), and (a_fin, $\tilde{\chi}_\mathrm{fin}$) for the nominal case $V_\mathrm{k} = 0.75\,\mathrm{km\,s^{-1}}$ and $T = 1 \times 10^5$ yr. The subscript 'fin' indicates the value at the end of a simulation. Fig. 7 shows the distributions in (a_fin, e_fin^2) for two other combinations of V_k and T; the distributions of $\cos I_\mathrm{fin}$ and $\tilde{\chi}_\mathrm{fin}$ are essentially the same as in the nominal case.

The retained comets with relatively small a remain well described by a thermal eccentricity distribution; that is, at a given a, they are uniformly distributed in e^2, with perhaps a moderate enhancement of the number of comets with low eccentricities. For $a \gtrsim 10^4$ au,

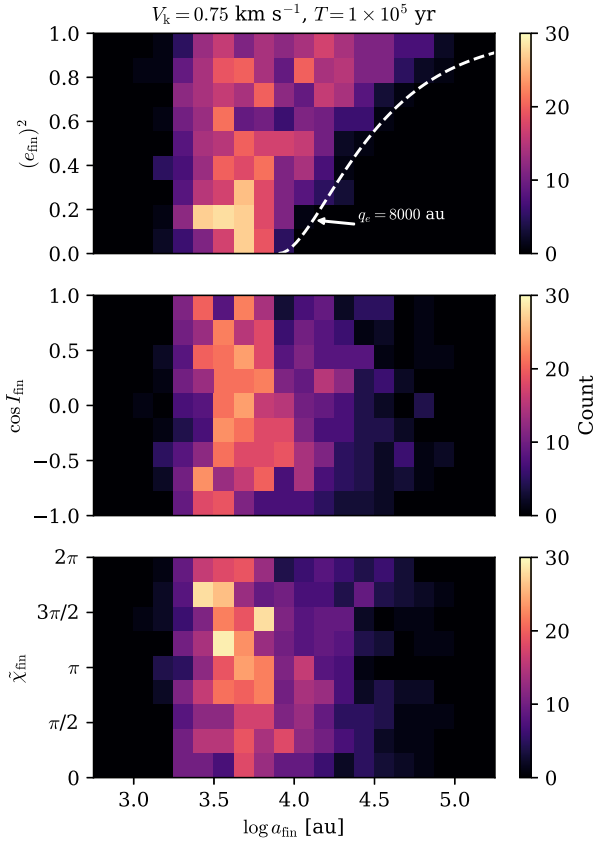

Figure 6. Top panel: 2D histogram of retained comets in the (a, e^2) plane for $V_k = 0.75\,\mathrm{km\,s^{-1}}$ and $T = 1 \times 10^5$ yr. The dashed white curve is a curve of constant $q = 8000$ au. Middle panel: the same in the $(a, \cos I)$ plane. Bottom panel: the same in the $(a, \tilde{\chi})$ plane.

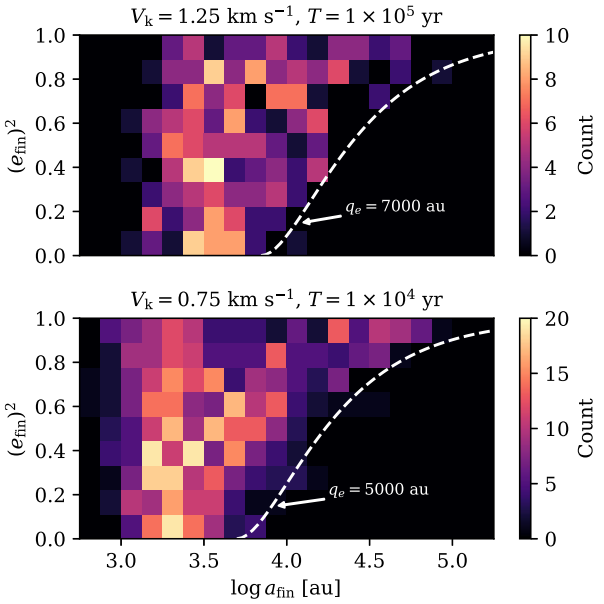

Figure 7. Top panel: the same as the top panel of Fig. 6, but for $V_k = 1.25\,\mathrm{km\,s^{-1}}$. Bottom panel: the same, but for $V_k = 0.75\,\mathrm{km\,s^{-1}}$ and $T = 1 \times 10^4$ yr.

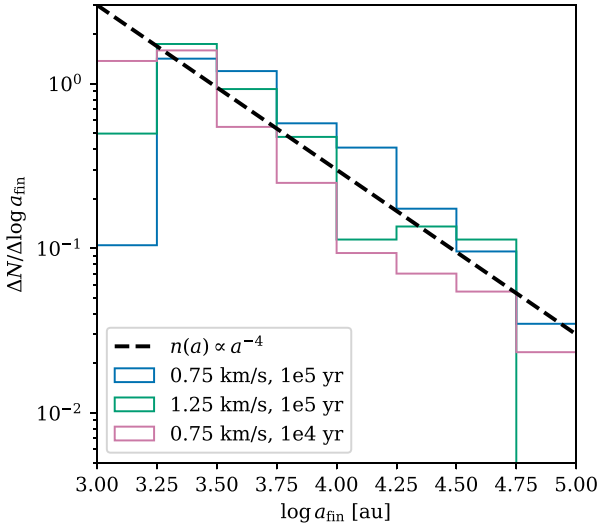

Figure 8. Incremental distributions of the final semimajor axis of retained comets with final $q \leq 1000$ au for different V_k and T values. The dashed line indicates a power-law density profile $n(a) \propto a^{-4}$.

only objects with high eccentricities are retained, and the minimum eccentricity increases with a. This is because objects at large distances are more likely to survive if the kick occurs whilst they are near periastron. For a given experiment, the 'edge' of the survivors' distribution can be approximated as a curve of constant $q \equiv q_e$, the location of which may be somewhat sensitive to V_k and T. For $q \leq q_e$, the eccentricities of comets follow a truncated thermal distribution. The inclinations and apsidal angles of retained comets are isotropically distributed (uniform in $\cos I$ and $\tilde{\chi}$) at all a.

The initial cometary orbits followed a power-law density profile $n(a) \propto a^{-\alpha}$ with $\alpha = 7/2$. The preferential retention of comets with small q implies that the distribution function of retained comets $f(L, J)$ is not a pure power law in L (or a). However, from equations (8) and (9), only the value of f on the surface $J = J_{cr}$ determines the comet injection rate. We characterize f in this limit by examining the radial distribution of survivors with periastron distances $q_{fin} \leq 1000$ au. Fig. 8 shows that, over a large range of a_{fin}, the survivors follow power-law density profiles with $\alpha \approx 4$. This represents a slightly more concentrated profile than the initial state.

Overall, we find that the distribution of retained comets in our simulations can be well approximated as (cf. equation 16)

$$f(L, J) = \begin{cases} C' N_c' (L/L_1)^{3-2\alpha}, & L_1 \leq L \leq L_e; \\ C' N_c' (L/L_1)^{3-2\alpha}, & 0 \leq J \leq J_e(L),\ L_e \leq L \leq L_2; \\ 0, & \text{else}; \end{cases} \tag{33}$$

where

$$J_e(L) = L_e \left(2 - \frac{L_e^2}{L^2}\right)^{1/2}, \qquad L_e = (GMq_e)^{1/2} \tag{34}$$

The quantity N_c' is the total number of retained comets, i.e. $N_c' = f_{ret} N_c$. This is the same distribution function used in Section 2 (equation 16), but it is truncated for $a \geq q_e$ ($L \geq L_e$) and $q \leq q_e$ ($J \leq J_e(L)$). The normalization factor C' is a complicated function of L_1, L_2, and α, but it reduces to equation (17) in the limit $L_0 \to L_2$. Numerically, C' is only a factor of a few smaller than C for a given α.

3.4 Revised bombardment rate

Based on our characterization of the distribution function, the major assumptions made by HT86 also hold for the retained comets in our simulations. We can therefore apply equations (8) and (9) as appropriate to calculate the comet accretion rate for the WD.

We evaluate the comet accretion rate after stellar mass-loss for the illustrative case $T = 1 \times 10^5$ yr and $V_k = 0.75\,\mathrm{km\,s^{-1}}$. The remnant XOC contains $N_c' \simeq 0.1 N_c$ between $a_1' \simeq 2 \times 10^3$ au and $a_2' \simeq 8 \times 10^4$ au with $\alpha \simeq 4$. Using the HT86 formalism with $f(L, J)$ given by equation (33), we find

$$\dot{M}_Z \simeq 9 \times 10^6\,\mathrm{g\,s^{-1}} \left(\frac{f_{\rm acc} m_c}{10^{17}\,\mathrm{g}}\right)\left(\frac{f_{\rm ret} N_c}{10^{10}}\right). \tag{35}$$

This is lower than the accretion rate calculated in Section 2.1.4 (equation 20). However, it still falls well within the range of measurable WD accretion rates. We conclude that the dynamical effects of late-stage stellar evolution cannot entirely explain the absence of cometary pollution.

4 COMET DEFLECTION BY SURVIVING PLANETS

In Sections 2 and 3, we estimated the rate at which XOC comets are injected to within $q_{\rm cr} = r_{\rm tide}$ around a WD by the Galactic tide. However, the presence of remnant planetary systems around WDs could potentially alter the trajectories of incoming comets, preventing their accretion by the WD. In the Solar system, LPCs have a high probability of being diverted by Jupiter or Saturn during each perihelion passage (e.g. Fernández 1981). This 'Jupiter–Saturn barrier' has long been thought to reduce the flux of LPCs near Earth and, by extension, the rate of LPC impacts on the Sun. In this section, we investigate the conditions under which surviving planets would prevent pollution of the star by XOC comets.

4.1 Orbit-averaged interactions

We first consider the case where the periastron distance $q = a(1 - e)$ of an XOC comet is larger than the orbital semimajor axis of a perturbing planet (a_p). The planet–comet interaction may be averaged over the orbital motions of both bodies. This secular interaction gives rise to apsidal precession of the comet at a rate (e.g. Murray & Dermott 1999)

$$\left(\frac{\mathrm{d}\chi}{\mathrm{d}t}\right)_p = \frac{3}{8}\frac{m_p a_p^2}{M a^2}\frac{5(\hat{\boldsymbol{n}}\cdot\hat{\boldsymbol{n}}_p)^2 - 1}{(1-e^2)^2}\,\omega, \tag{36}$$

where m_p is the planet's mass and $\hat{\boldsymbol{n}}$ and $\hat{\boldsymbol{n}}_p$ are the comet's and planet's unit angular momentum vectors. The Galactic tidal field also induces apsidal precession (see equation 4).

Competition between the planetary and Galactic tidal perturbations imposes a maximum eccentricity $e_{\rm max}$ for the comet – or, equivalently, a minimum periastron distance $q_{\rm min}$. Several previous studies of closely related dynamical systems have demonstrated the existence of this maximum eccentricity (Fabrycky & Tremaine 2007; Liu, Muñoz & Lai 2015; Pichierri, Morbidelli & Lai 2017; Hamilton & Rafikov 2021). Its physical cause is rapid apsidal precession of the comet due to the planetary perturbation, which becomes important at small q; this, in turn, suppresses the resonant eccentricity driving from the Galactic tide. We can therefore estimate $e_{\rm max}$ by calculating the eccentricity for which the precession rates due to each perturbation are comparable in magnitude. This yields

$$1 - e_{\rm max} \sim \left(\frac{m_p a_p^2}{\rho_g a^5}\right)^{2/3} \tag{37}$$

or, in terms of periastron distance,

$$\begin{aligned} q_{\rm min} &= a(1 - e_{\rm max}) \\ &\sim 20\,\mathrm{au}\left(\frac{m_p}{M_J}\right)^{2/3}\left(\frac{a_p}{10\,\mathrm{au}}\right)^{4/3} \\ &\quad\times\left(\frac{\rho_g}{0.1\,\mathrm{M_\odot\,pc^{-3}}}\right)^{-2/3}\left(\frac{a}{10^4\,\mathrm{au}}\right)^{-7/3}. \end{aligned} \tag{38}$$

For a multiplanet system, the quantity $m_p a_p^2$ can be replaced with $K = \sum_p m_p a_p^2$, where the summation is taken over all planets.

For a given m_p and a_p, comets with sufficiently large a have $q_{\rm min} \lesssim a_p$, i.e. they will still cross the orbit of the planet. Thus, from equation (38), we see that planets with $m_p \gtrsim 1 M_J$ and $a_p \gtrsim 10$ au can repel incoming comets through orbit-averaged perturbations, but smaller or shorter period planets cannot.

4.2 Direct scattering

A comet passing through a planetary system may be scattered after encountering a planet. The majority of comets do not experience a close encounter, defined as occurring when the minimum separation between the comet and planet is smaller than the Hill radius of the planet ($\sim a_p[m_p/M]^{1/3}$). However, the energy received by the comet from a distant encounter ($\sim G m_p/a_p$) can still be comparable to its orbital binding energy ($\sim GM/a$). The ratio of these quantities,

$$\Lambda = \left(\frac{m_p}{M_J}\right)\left(\frac{\mathrm{M_\odot}}{M}\right)\left(\frac{a}{10^4\,\mathrm{au}}\right)\left(\frac{10\,\mathrm{au}}{a_p}\right), \tag{39}$$

is reminiscent of the Safronov number for planetesimal scattering. For $\Lambda \ll 1$, the comet receives a negligible kick and can undergo many repeated passages until it collides with the planet or star. For $\Lambda \gtrsim 1$, the comet may be ejected into interstellar space or captured in a short-period orbit. Either way, incoming comets with $\Lambda \gtrsim 1$ may be efficiently removed from the OC and no longer have their q reduced by the Galactic tide.

To corroborate the general picture presented above, we conducted N-body simulations of the passage of a near-parabolic comet through a planetary system with REBOUND. We considered a system containing a WD ($M = 0.6\,\mathrm{M_\odot}$) and a single planet of mass m_p, semimajor axis $a_p = 10$ au, and eccentricity $e_p = 0.2$ (typical of long-period exoplanets; e.g. Dawson & Murray-Clay 2013; Buchhave et al. 2018) The comet was treated as a massless test particle, initialized on an incoming near-parabolic orbit with barycentric semimajor axis $a = 2 \times 10^4$ au. We varied the comet's initial pericentre distance q, inclination I (relative to the planetary orbit), apsidal angle χ, and nodal angle Ω, as well as the planet's initial mean longitude λ_p. We considered values of the planet-to-star mass ratio $\mu = m_p/M$ of 10^{-6}, 10^{-5}, 10^{-4}, and 10^{-3}. These correspond to Λ values from 0.002 to 2.0.

For each combination of m_p and q, we conducted 45 000 REBOUND simulations, sampling $\cos I$, χ, Ω, and λ_p from a uniform grid over their full range of possible values. We also sampled 30 uniformly spaced q values on the interval $[0.005, 1.5]a_p$. Each run lasted a time $2T_q$, where T_q is the time it would take for the comet to travel from its initial position to periastron along its initial orbit. We used the IAS15 integrator in REBOUND.

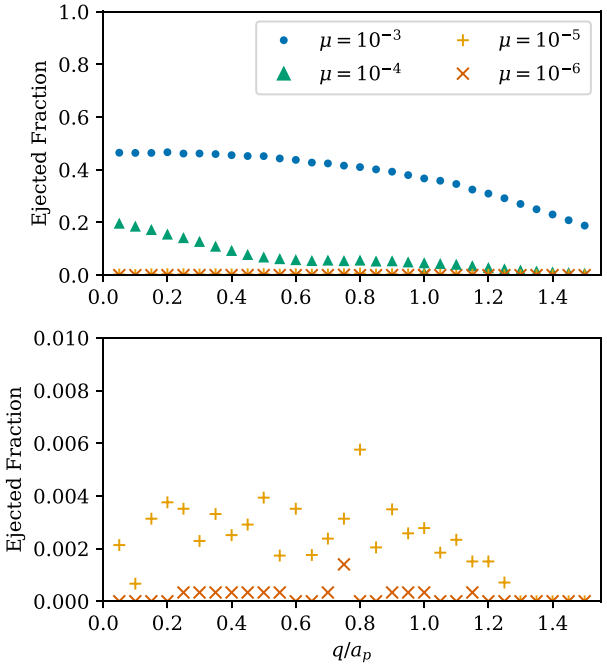

Figure 9. Top panel: fraction of comets ejected from a single-planet system as a function of $\mu = m_p/M$ and q/a_p. The comets are initialized with $a = 2 \times 10^4$ au. Bottom panel: a vertical zoom on the data for $\mu = 10^{-5}$, 10^{-6}.

We determined the fate of each comet in post-processing. We assume that the comet is ejected if its final barycentric distance is at least $2a_p$ and its final osculating orbit is either hyperbolic or elliptical with apoastron distance $Q > 0.8$ pc. If neither condition was met, the comet was considered bound. In reality, the bound comets would either return to the OC or be captured on a shorter period orbit. Either way, their ultimate fates are not determined in our simulations.

Fig. 9 shows the fraction of incoming comets that are ejected as a function of initial q. These results are averaged over all other initial conditions (i.e. over the orientation of the comet's orbit). The ejected fraction generally increases with increasing μ and decreasing q. For $\mu = 10^{-6}$ and 10^{-5}, only a very small fraction of comets are ejected, if any. For $\mu = 10^{-4}$, the fraction increases from 0.005 at $q/a_p = 1.5$ to 0.19 at $q/a_p = 0.005$. For $\mu = 10^{-3}$, it increases from 0.18 to 0.45 over the same range.

Figs 10 and 11 show cumulative distributions of the final semimajor axes of comets that remained bound after encountering the planet. This distribution is necessary to determine the fraction of bound comets that are continually pushed inward by the Galactic tide over successive periastron passages. We focus on the cases $\mu = 10^{-3}$ and 10^{-4}, since the effect of the planet is negligible for smaller μ.

For $\mu = 10^{-3}$, 60–80 per cent of bound comets experience a reduction in semimajor axes by more than a factor of 2. A greater fraction of bound comets belong to this subset as q decreases. Comets with $a_{fin} \lesssim 3 \times 10^3$ au are decoupled from the Galactic tide (tidal torque $\propto a^2$) and no longer have their q reduced between successive periastron passages. In the case of $\mu = 10^{-4}$, less than 20 per cent of bound comets experienced a significant reduction of the semimajor axis. Moreover, almost none had $a_{fin} \lesssim 3 \times 10^3$ au. These results confirm qualitative expectations based on the value of Λ.

The statistical outcomes of near-parabolic encounters between a test particle and a star–planet system would be worthwhile to study in a future work. For the purposes of this work, we conclude that a

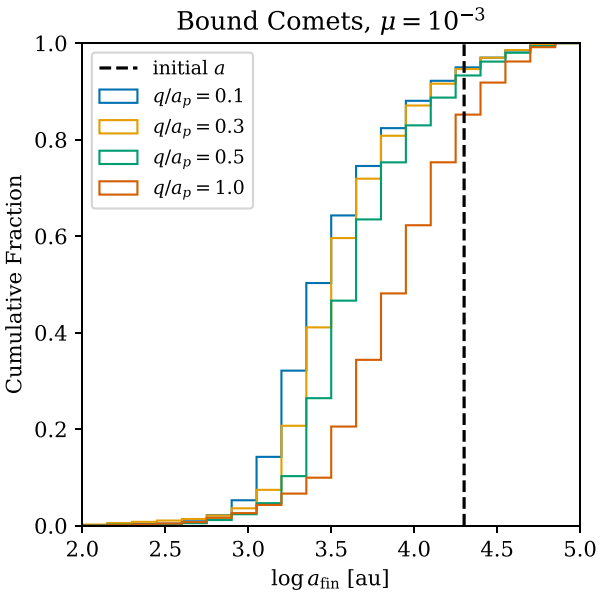

Figure 10. Cumulative distribution of the final semimajor axes of comets on bound orbits after a parabolic encounter with a WD–planet system with $a_p = 10$ au and $\mu = 10^{-3}$. The vertical dashed line indicates the comet's initial semimajor axis ($a = 2 \times 10^4$ au).

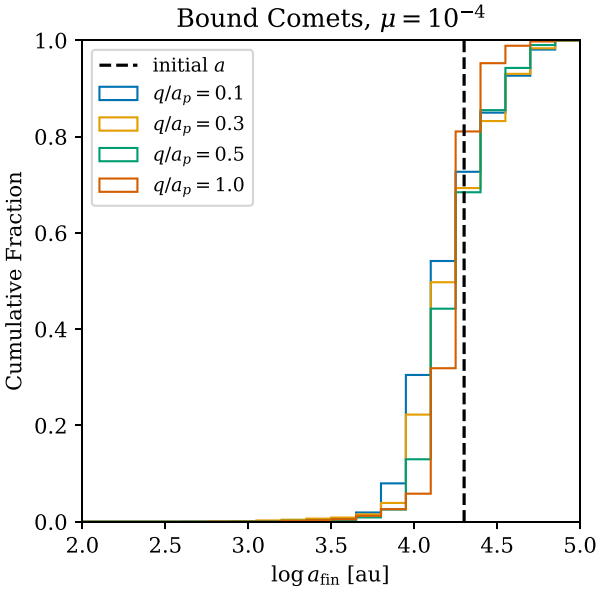

Figure 11. The same as Fig. 10 with $\mu = 10^{-4}$.

planet with $\Lambda \gtrsim 1$ likely creates a dynamical barrier to LPCs with $q \lesssim a_p$. In the next section, we estimate the reduction of the tidal disruption rate of LPCs from this effect.

4.3 Reduced comet injection rate

OC comets interacting with Jupiter or Saturn have $\Lambda \gtrsim 1$. Consequently, it is generally thought that the Jovian planets reduce the overall flux of LPCs in the innermost part of the Solar system. However, to our knowledge, previous studies have not quantified the expected reduction of the LPC flux at very small q due to scattering by planets. This is necessary to calculate the comet accretion rate of

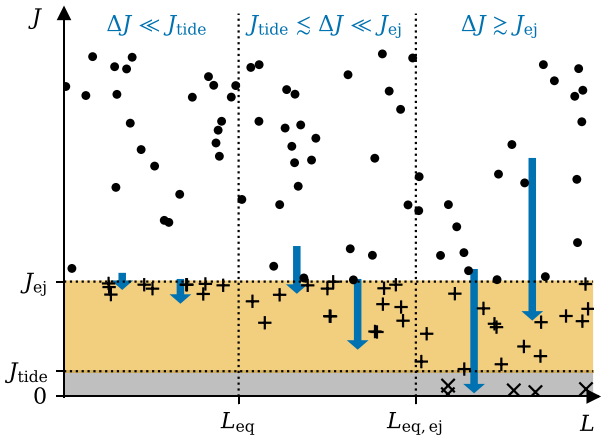

Figure 12. Schematic depiction of the modified loss cone theory in the presence of a planetary barrier. The 'tidal disruption' loss cone is shaded in grey, whilst the 'ejection loss cone' is shaded in light orange. Comets with $L \lesssim L_{\rm eq,ej}$ are predominantly ejected by the planet (plus signs), whilst those with $L \gtrsim L_{\rm eq,ej}$ are either ejected or tidally disrupted by the WD (crosses). Note that the size of $J_{\rm tide}$ relative to $J_{\rm ej}$ is exaggerated for visual clarity.

a planet-hosting WD. Incidentally, it also relates to the production of Sun-grazing comets from the OC (e.g. Novski et al. 2012; Fernández, Lemos & Gallardo 2021) and observed exocomets around planet-hosting main-sequence stars (e.g. Ferlet et al. 1987).

Suppose that a comet has a probability $p_{\rm ej}$ of being ejected during each passage through the remnant planetary system of a WD. The probability of being ejected after exactly k passages is

$$p(k) = p_{\rm ej}(1-p_{\rm ej})^{k-1}, \tag{40}$$

and the expected passage number on which ejection occurs is

$$\langle k\rangle = \sum_{k=1}^{\infty} k p(k) = \frac{1}{p_{\rm ej}}. \tag{41}$$

The numerical experiments presented in Section 4.2 demonstrated that $p_{\rm ej}$ approaches 0.5 for planets with $\Lambda \gtrsim 1$. Therefore, in the presence of this dynamical barrier, the cumulative comet ejection fraction of LPCs with $q \lesssim a_{\rm p}$ is 0.5 after the first periastron passage, 0.75 after the second, and so on.

For $r_{\rm tide} \leq q \lesssim a_{\rm p}$, comets can be either injected by Galactic tides to smaller q (perhaps leading to tidal disruption) or ejected into interstellar space by the planet. The competition between these processes determines the comet accretion rate of the WD in the presence of the planet. A similar effect in dense star clusters with central black holes has been dubbed 'loss cone shielding' by Teboul, Stone & Ostriker (2022).

We quantify the amount by which the accretion rate is reduced via a straightforward modification of the loss cone theory, illustrated schematically in Fig. 12. We define an 'ejection loss cone' with $J_{\rm cr} = (2GMa_{\rm p})^{1/2} \equiv J_{\rm ej}$; in general, we have $J_{\rm ej} \gg J_{\rm tide} = (2GMr_{\rm tide})^{1/2}$. The two loss cones overlap, with the ejection loss cone covering a much larger region of phase space. For a comet with relatively small a (L), such that the change of its angular momentum per orbit ΔJ is smaller than $J_{\rm ej}$, the ejection loss cone is empty; for a comet with larger a such that $\Delta J \gtrsim J_{\rm ej}$, this loss cone is filled. The transition semimajor axis is

$$a_{\rm eq,ej} \simeq 0.38\left(\frac{M^2 a_{\rm p}}{\rho_{\rm g}^2}\right)^{1/7}, \tag{42}$$

which exceeds $a_{\rm eq}$ (see equation 10) by a factor $(a_{\rm p}/r_{\rm tide})^{1/7}$; we also define the corresponding value $L_{\rm eq,ej} \equiv (GMa_{\rm eq,ej})^{1/2}$. Because the tidal-disruption loss cone is nested deep inside the ejection loss cone, comets with $L \lesssim L_{\rm eq,ej}$ are mostly ejected before they reach the tidal radius ($J = J_{\rm tide}$). On the other hand, those with $L \gtrsim L_{\rm eq,ej}$ can reach $J \leq J_{\rm tide}$ in a single orbit, avoiding ejection. The accretion rate onto the WD from comets in the filled ejection loss cone is therefore given by the steady-state number of comets with $J \lesssim J_{\rm tide}$ (at a given L) divided by their orbital period $P(L)$ – the same as equation (9) with $J_{\rm cr} = J_{\rm tide}$. Thus, in the presence of a strong planetary barrier, the total comet bombardment rate on the WD is

$$\Gamma_{\rm tot}^{\rm (pl)} \simeq \int_{L_{\rm eq,ej}}^{L_2} \Gamma_{\rm f}(L)\,{\rm d}L \sim L_{\rm eq,ej}\Gamma_{\rm f}(L_{\rm eq,ej}). \tag{43}$$

This can be compared to the bombardment rate without a planetary barrier, $\Gamma_{\rm tot}^{\rm (no\ pl)} \sim L_{\rm eq}\,\Gamma_{\rm f}(L_{\rm eq})$ (see equation 7). Using the relations $\Gamma_{\rm f}(L) \propto f(L, J_{\rm tide})/L^3$ (equation 9) and $f \propto L^{3-2\alpha}$ (equation 33), we find

$$\frac{\Gamma_{\rm tot}^{\rm (pl)}}{\Gamma_{\rm tot}^{\rm (no\ pl)}} \sim \left(\frac{L_{\rm eq,ej}}{L_{\rm eq}}\right)^{1-2\alpha} = \left(\frac{r_{\rm tide}}{a_{\rm p}}\right)^{(2\alpha-1)/14}. \tag{44}$$

For typical values $2 \leq \alpha \leq 4$, this ratio is much less than unity unless $a_{\rm p}$ is close to $r_{\rm tide}$. For example, taking $\alpha = 7/2$, we have

$$\frac{\Gamma_{\rm tot}^{\rm (pl)}}{\Gamma_{\rm tot}^{\rm (no\ pl)}} \sim \left(\frac{r_{\rm tide}}{a_{\rm p}}\right)^{3/7} \approx 0.05\left(\frac{r_{\rm tide}}{0.01\,{\rm au}}\right)^{3/7}\left(\frac{a_{\rm p}}{10\,{\rm au}}\right)^{-3/7}. \tag{45}$$

We conclude that planets with $\Lambda \gtrsim 1$ and $a_{\rm p} \gg r_{\rm tide}$ are capable of significantly reducing the comet accretion rate of a WD. Notice that the planetary barrier reduces the accretion rate more severely when the XOC is more centrally concentrated (greater α).

5 DISCUSSION

We find that both late-stage stellar evolution and the presence of a surviving planetary system can reduce the rate at which XOC comets bombard a central WD. The primary cause of the reduction is the ejection of comets into interstellar space. This can occur either during stellar mass-loss or after a scattering event from one of the planets. The simplified model XOC described in Section 2 produces a metal accretion rate given by

$$\dot{M}_Z \sim 10^8\,{\rm g\,s^{-1}}\,f_{\rm acc}\left(\frac{m_{\rm c}}{10^{17}\,{\rm g}}\right)\left(\frac{N_{\rm c}}{10^{11}}\right),$$

where $N_{\rm c}$ refers to the number of comets in the cloud with $a > 10^4$ au and $m_{\rm c}$ is the typical mass of a comet. The results of the previous two sections can be incorporated into this estimate by multiplying the right-hand side of equation (5) by two additional factors, $f_{\rm ret}$ and $f_{\rm bar}$. These two factors account for the retention of comets through stellar evolution and the planetary barrier effect. We found that each of these factors is typically ≈0.01–0.1, depending on the magnitude of WD kicks ($f_{\rm ret}$) and the orbital radii of the surviving planets ($f_{\rm bar}$). Neither process acting alone is sufficient to reduce the comet accretion rate below the observational detection threshold of $\sim 10^5\,{\rm g\,s^{-1}}$. However, both processes operating in parallel could reduce the accretion rate below the observational constraints. An inefficient accretion process ($f_{\rm acc} \lesssim 1$) would further reduce $\dot{M}_Z$.

The factors $f_{\rm ret}$ and $f_{\rm bar}$ are expected to vary between systems. A subset of polluted WDs could therefore be accreting marginally detectable amounts of cometary debris ($\sim 10^5$–$10^6\,{\rm g\,s^{-1}}$). Given that only a few dozen polluted WDs have been characterized in detail, these may have gone unnoticed to date. A confounding factor is that

comet-hosting WDs may also possess populations of intrinsically 'rocky' bodies, such as exo-asteroids. Many authors have argued that these are the main parent-body population for the observed pollution in many systems (Jura 2006, 2008; Debes et al. 2012; Mustill et al. 2018; Smallwood et al. 2018, 2021; O'Connor et al. 2022; Trierweiler et al. 2022). If exo-asteroids are accreted by the WD at a much greater rate than icy bodies on average, then the contribution from exocomets to the atmospheric chemical abundances may be obscured.

5.1 Comparison with related works

Alcock et al. (1986) and Parriott & Alcock (1998), respectively, carried out early studies of the dynamical effects of symmetric and asymmetric mass-loss on an XOC. They used a parametrized prescription for the mass-loss and natal kick similar to ours. The fraction of comets that remain bound to the WD in their simulations agrees with our result in order of magnitude.

Veras et al. (2014) conducted *N*-body simulations of the evolution of an XOC during late-stage stellar evolution for host stars of several different masses. Their simulations included the Galactic tidal field and random stellar flybys but did not include a possible surviving planetary system or a natal kick on the host. Despite this, Veras, Shannon & GänsickeVeras et al. found a lower comet accretion rate compared to our analytical estimate: specifically, they found that a fraction $\sim 10^{-5}$ of comets were accreted by the WD over 10 Gyr. When assuming an $\sim 1 M_{\oplus}$ cloud, this corresponds to an average accretion rate of $\dot{M}_Z \sim 10^5\,\mathrm{g\,s^{-1}}$; this rate is comparable to the observational detection limit and far below the value $\dot{M}_Z \sim 10^8\,\mathrm{g\,s^{-1}}$ we estimated analytically. The difference most likely arises because Veras, Shannon & GänsickeVeras et al. considered OC comets initially distributed between 10^4 and 10^5 au on the MS, rather than from 10^3 to 10^5 au as in our case. A larger fraction of the comets would have been lost during stellar mass-loss in their simulations than in ours, reducing the subsequent accretion rate of the WD.

Stone et al. (2015) studied the direct injection of cometary material to $\sim$10 au distances as a result of the natal kick of the WD. They calculated the change of comet orbits using an impulse approximation throughout the cloud. Specifically, they assumed that the kick is imparted in the final few 10^4 yr of stellar evolution, after the vast majority of mass-loss has occurred through an isotropic wind. This may be more realistic than our assumption that the mass-loss and kick occur simultaneously, and the distribution function of surviving comets would likely be different. However, Stone, Metzger & LoebStone et al. did not discuss the long-term pollution of the central WD in their study.

Finally, Caiazzo & Heyl (2017) calculated the orbital evolution of XOC comets during isotropic stellar mass-loss, using a realistic time-dependent mass-loss rate from MESA. They did so by constructing an approximate interpolation scheme between the adiabatic and impulsive mass-loss regimes. This scheme, or alternatively that of Veras et al. (2011), could be adapted to include a time-dependent kick acceleration on the host star in order to predict the distribution function of surviving comets more accurately. This is outside of the scope of this paper but would be useful to investigate in future work.

5.2 Comets and habitability of WD planets

The discovery of surviving short-period planets around WDs (e.g. Vanderburg et al. 2020) has prompted speculation and investigation regarding their habitability. Particular emphasis has been placed on hypothetical Earth-sized rocky planets (Kaltenegger et al. 2020, and references therein). Comet impacts are integral to the question of planetary habitability in the Solar system and elsewhere. Comets can deliver the chemical ingredients of terrestrial life – water and other volatile compounds – to worlds formed inside the condensation lines of these species in the birth nebula (e.g. Owen & Bar-Nun 1995; Dauphas, Robert. Fran & Bernard 2000; Dauphas 2003). Impact events by either comets or asteroids are a potential cause of mass extinctions or climatic shifts on our own planet (e.g. Alvarez et al. 1980; Kent et al. 2003).

Here, we focus on the ability of comets to deliver volatile substances. The traditional habitable zone around an evolved, cool WD occurs at $a \approx 0.01$ au (Agol 2011). Either dynamical migration (Veras & Gänsicke 2015; Muñoz & Petrovich 2020; O'Connor, Liu & Lai 2021; Stephan, Naoz & Gaudi 2021) or second-generation formation (Bear & Soker 2015; van Lieshout et al. 2018) is required for rocky planets to exist there. Such planets are prone to volatile depletion through intense tidal heating (Barnes & Heller 2013) or ultraviolet irradiation (Lin et al. 2022). Delivery of XOC comets to short-period orbits and subsequent collisions with planets could, in principle, replenish the volatiles.

The habitable zone and the Roche limit occur at roughly the same distances around an old WD ($\simeq$0.01 au), notwithstanding extra heating processes such as tidal friction (Becker et al. 2023). Therefore, the rate at which a short-period planet captures cometary material is at most of the order of the accretion rate of the host star. The fraction of material captured by a planet via direct impacts depends on its accretion cross-section and the comet's orbital geometry (Torres et al. 2021; Seligman et al. 2022b). A planet near the Roche limit may be able to capture additional material from a circumstellar debris disc (van Lieshout et al. 2018).

Based on the non-detection of comet-like debris in polluted WD atmospheres, we place a characteristic upper bound of $\dot{M}_Z \approx 10^5\,\mathrm{g\,s^{-1}}$ for the time-averaged accretion rate of cometary material onto hypothetical short-period planets. This constrains the total amount of volatiles that these planets can acquire from comet impacts over their lifetimes. For example, if the mass fraction of water ice in a typical comet is $X_{\mathrm{H_2O}}$, then the planet can accrete water from comets at a maximum rate

$$\dot{M}(\mathrm{H_2O}) \approx 10^{21}\,\mathrm{g\,Gyr^{-1}} \left(\frac{\dot{M}_Z}{10^5\,\mathrm{g\,s^{-1}}}\right)\left(\frac{X_{\mathrm{H2O}}}{0.3}\right). \quad (46)$$

Based on theoretical WD cooling models, Kozakis, Kaltenegger & Hoard (2018) found that a planet orbiting a 0.6-$\mathrm{M}_{\odot}$ WD at $a =$ 0.01 au can remain habitable for [4, 9] Gyr. For $\dot{M}_Z = 10^5\,\mathrm{g\,s^{-1}}$ and $X_{\mathrm{H_2O}} = 0.3$, this implies up to $[4, 9] \times 10^{21}$ g of cometary water may be accreted by such a planet during its habitable lifetime. This is much less than the mass of Earth's oceans, but it is comparable to that of Mars' ice caps (Christensen 2006). Similarly, for a bulk nitrogen mass fraction $X_{\mathrm{N}} = 0.015$ in a Halley analogue (Jessberger et al. 1988), some $[2, 5] \times 10^{20}$ g of N could be delivered in the same time-frame. This would amount to [4,10] per cent of the total mass of Earth's atmosphere. In short, accretion from comets at the level of current observational constraints could provide a rocky planet in the habitable zone of a WD with a significant global budget of volatile compounds.

5.3 Caveats

5.3.1 Analytical calculation of the injection rate

The comet injection rate calculated by HT86 only accounted for the vertical component of the Galactic tide. The radial and tangential components are smaller by an order of magnitude. The dynamics of a

comet under the vertical Galactic tide is an instance of the evolution of a binary in an axisymmetric external potential (Hamilton & Rafikov 2019). The inclusion of weaker non-axisymmetric components tends to excite extreme orbital eccentricities (e.g. Naoz et al. 2013; Pejcha et al. 2013). Indeed, Fouchard et al. (2006) found that the radial tidal force slightly increases the comet delivery rate in the Solar system at $q \sim$ few au. Similar effects may enhance the accretion rate of a WD. It would be worthwhile to generalize the calculation of the injection rate in HT86 to the non-axisymmetric case in future work.

Throughout this work, we have assumed that Galactic tides and stellar flybys operate on XOC comets with a known distribution function. We argued that stellar flybys have a subdominant contribution to the comet injection rate, although they are important in shaping the distribution function of XOC comets (see HT86). However, previous numerical calculations have demonstrated that the injection rate can deviate from our prediction when Galactic tides and flybys operate simultaneously (Rickman et al. 2008; Fouchard et al. 2011a, b). Considering a fiducial OC model similar to ours (with $\alpha = 7/2$, $a_1 = 3000$ au, and thermal eccentricities), Rickman et al. (2008) and Fouchard et al. (2011a) calculate the LPC flux at $q < 5$ au to be $\sim$0.2–0.4 yr^{-1} per 10^{11} OC objects. Our model predicts a flux at $q < 4$ au of $\sim 3\,\mathrm{yr}^{-1}$ per 10^{11} OC objects; evidently, our model overestimates the numerical result by a factor of $\sim$10.

This discrepancy may be due to our simplistic treatment of the transition between the empty and filled loss cone regimes. Specifically, we have assumed that the loss cone is entirely filled at $a = a_{\rm eq}$, which leads to an overestimate of the magnitude of the 'peak' in the differential injection rate $\Gamma(L)\,\mathrm{d}L$. However, even if the quantity in equation (20) is overestimated by a factor of 10, the predicted accretion rate $\dot{M}_Z$ would still be orders of magnitude *above* the observational detection limit. Moreover, the scaling laws predicted by the HT86 formalism are valid despite the magnitude of the flux. Thus, our main conclusions are not affected by our approximate analytical estimate.

5.3.2 Isotropy and scale of XOCs

We have assumed that the XOC has a spherically symmetric structure throughout this work. Here, we briefly qualify this assumption to order-of-magnitude accuracy.

The outer OC surrounding the Solar system is likely mildly anisotropic due to the anisotropy of the Galactic tidal field (e.g. HT86). The inner cloud is likely highly anisotropic, due to its presumed dynamical relationship with the giant planets (e.g. Duncan et al. 1987). As we demonstrated in Section 3, comets in the inner OC are preferentially retained through late stellar evolution. Therefore the surviving XOC of a young WD may inherit the same degree of anisotropy, modulo the effects of asymmetric mass-loss. It is feasible to incorporate this anisotropy in our model by truncating the fiducial spherical distribution function for a range of orientations. It would then be straightforward to calculate the comet injection rate from such a cloud following similar steps to HT86.

On the other hand, the degree of anisotropy in a cloud would be reduced over time following post-MS orbital expansion. This is because the expansion of cometary orbits makes them more susceptible to diffusion driven by weak stellar flybys. Based on theoretical models for the Solar system, a surviving XOC around a WD would become dynamically relaxed around a cooling age of $\sim$1 Gyr.

Another underlying assumption of our discussion is that XOCs have the same characteristic size as the solar OC. However, the size of an XOC is a function of the architecture and initial conditions of the inner planetary system and the density of the galactic environment in which it formed (Fernández 1997). If the progenitors of single WDs form in denser environments or have more compact or less massive planetary systems, then their XOCs would be smaller and less susceptible to ejection during stellar mass-loss. On the other hand, their comets would be less prone to injection by Galactic tides when the host star resides within a less dense environment.

5.3.3 Composition of cometary nuclei

We have assumed throughout this work that cometary debris in a WD atmosphere would have bulk elemental abundances similar to Halley's comet (cf. Jura 2006; Xu et al. 2017). However, cometary nuclei within the Solar system display diverse compositions (e.g. A'Hearn et al. 2012; Cochran et al. 2015; Bockelée-Morvan & Biver 2017). Notably, some have sub-solar C abundances on par with those measured in polluted WDs (Seligman et al. 2022b). It is plausible that some WDs are polluted by relatively volatile-poor comets.

The issue of composition is also related to the question of XOC scale raised in Section 5.3.2. A comet in a relatively compact XOC ($\lesssim 10^3$ au) would be subjected to intense heating during the host's post-MS evolution, possibly leading to loss of volatiles by sublimation. In that case, the material that subsequently pollutes the WD may be dominated by refractory elements, perhaps rendering it indistinguishable from other rocky debris (Zhang, Liu & Lin 2021). Levine et al. (2023) have addressed this by modelling the thermal evolution of OC objects around post-MS stars. They find that objects in the inner OC up to $\sim$1 km in size may become depleted in hypervolatiles (compounds with low sublimation temperatures, such as H_2, CO, and N_2) due to post-MS thermal processing. However, hypervolatiles constitute only a moderate fraction of the total mass in typical cometary nuclei; compounds with relatively high sublimation temperatures (e.g. H_2O, CO_2, NH_3) are often present alongside hypervolatiles in similar amounts (e.g. Biver et al. 2022, and references therein). Observations of polluted WDs reveal only the bulk elemental abundances of parent bodies, rather than the abundances of individual compounds. Thus, it is plausible that the chemical signature of an XOC object in a WD atmosphere would approximately reflect its primordial bulk composition, despite post-MS thermal processing.

6 CONCLUSION

We have studied dynamical processes operating on XOCs in relation to the rate at which LPCs are accreted by WDs. Our investigation has been informed by the observations that polluted WD atmospheres are typically depleted in volatile heavy elements. Our main conclusions are as follows:

(i) Adapting the loss cone theory of comet injeciton by the Galactic tide for the OC (HT86) we show that a WD would accrete cometary debris from a Solar-system-like XOC at a rate comparable to the typical total accretion rates observed in polluted systems. Assuming the composition of Halley's comet is representative of XOC objects, volatile elements would be readily observable in the WD's atmosphere in this scenario. This conclusion is insensitive to the radial distribution of comets, pro-

vided that the inner boundary of the cloud lies between 10^3 and 10^4 au.

(ii) Post-MS stellar mass-loss, including a possible natal kick imparted to a WD, causes a majority of XOC comets to be ejected as free-floating bodies. The fraction of comets retained by a newborn WD is sensitive to the kick speed but insensitive to the time-scale of stellar mass-loss (within a realistic range). Based on current constraints on the typical WD kick, single WDs retain between 1 and 30 per cent of XOC comets. The orbital distribution function of the survivors is modified to a moderate degree.

(iii) The presence of a surviving planetary system around a WD may reduce the rate at which comets fall to the Roche limit around a WD. Orbit-averaged perturbations from the planets on the comet's orbit can prevent comets interior to $\sim 10^4$ au from reaching small periastron distances under the influence of the Galactic tide (see Section 4.1). More importantly, direct scattering can cause up to $\sim$50 per cent of comets to be ejected on hyperbolic orbits, provided that the planet's mass $m_{\rm p}$ and semimajor axis $a_{\rm p}$ satisfy (see equation 39)

$$\Lambda = \frac{m_{\rm p}}{M}\frac{a}{a_{\rm p}} \gtrsim 1,$$

where M is the WD's mass and a is the comet's semimajor axis. Using a modified loss cone theory, we show that the presence of a 'planetary barrier' can significantly reduce the fraction of comets that reach the Roche limit (see Section 4.2).

We find that stellar mass-loss alone cannot sufficiently reduce the comet accretion rate to prevent observational detection of accreted volatiles. Therefore, to explain the dearth of detected volatiles in WDs, we suggest that a large fraction of polluted single WDs possess surviving planets with $\Lambda \gtrsim 1$ (with respect to a 'standard' XOC size $\sim 10^4$ au). Planets that avoided engulfment during post-MS evolution would orbit at distances $\gtrsim$5 au (e.g. Mustill & Villaver 2012). In order to block incoming comets effectively at this distance, the mass ratio of the planet relative to the WD must be $\gtrsim 10^{-3}$. This suggests that the surviving planets have typical masses $\gtrsim 0.6 M_{\rm J}(M/0.6\,{\rm M}_\odot)$. This inference is consistent with (i) observationally inferred giant-planet occurrence rates around A- and F-type MS stars (e.g. Johnson et al. 2010; Reffert et al. 2015; Jones et al. 2016; Ghezzi et al. 2018) and (ii) indirect chemical evidence for the presence of evaporating giant planets around a large fraction of young WDs (Schreiber et al. 2019). Our prediction is testable in the near term through planet searches targeting WDs using direct imaging (Brandner, Zinnecker & Kopytova 2021; Mullally et al. 2022), astrometry (Sanderson, Bonsor & Mustill 2022), and microlensing (Blackman et al. 2021).

The absence of volatile-enriched pollution among WDs has ramifications on the habitability and surface conditions of (hypothetical) short-period rocky planets orbiting these stars. Assuming that the accretion rate of cometary debris by such a planet is equal to the observational detection limit for the accretion rate of comets in the WD ($\sim 10^5\,{\rm g\,s^{-1}}$), global water and nitrogen budgets similar to present-day Mars and Earth, respectively, can both be achieved on Gyr time-scales.

Near the completion of this work, we learnt of a similar study being carried out by D. Pham and H. Rein. They are developing numerical techniques to study the long-term orbital evolution of a large ensemble of XOC comets under the same dynamical effects we have considered (D. Pham & H. Rein, private communication). Their approach is complementary to ours and will help to validate our analytical results.

ACKNOWLEDGEMENTS

We thank Juliette Becker, Boris Gänsicke, Chris Hamilton, Garrett Levine, Siyi Xu, and Ben Zuckerman for helpful discussions, as well as the organizers and participants of the KITP program *White Dwarfs as Probes of the Evolution of Planets, Stars, the Milky Way and the Expanding Universe* in Fall 2022. We also thank the anonymous referee for their helpful comments and suggestions.

This work has been supported in part by National Science Foundation Grants Nos PHY-1748958 and AST-2107796, as well as the Heising-Simons Foundation and the Simons Foundation (216179, LB). CEO gratefully acknowledges a Space Grant Graduate Research Fellowship from the New York Space Grant Consortium. DZS acknowledges financial support from NSF Grant No. AST-2107796, NASA Grant No. 80NSSC19K0444, and NASA Contract NNX17AL71A.

This work has made use of NASA's Astrophysics Data System and of the software libraries MATPLOTLIB (Hunter 2007), NUMPY (Harris et al. 2020), and SCIPY (Virtanen et al. 2020).

DATA AVAILABILITY

The data underlying this article will be shared on reasonable request to the corresponding author.

REFERENCES

A'Hearn M. F. et al., 2012, ApJ, 758, 29
Agol E., 2011, ApJ, 731, L31
Alcock C., Fristrom C. C., Siegelman R., 1986, ApJ, 302, 462
Alvarez L. W., Alvarez W., Asaro F., Michel H. V., 1980, Science, 208, 1095
Ambartsumian V. A., 1937, Astron. Zh., 14, 207
Anguiano B. et al., 2020, AJ, 160, 43
Barnes R., Heller R., 2013, Astrobiology, 13, 279
Barstow M. A., Barstow J. K., Casewell S. L., Holberg J. B., Hubeny I., 2014, MNRAS, 440, 1607
Bauer E. B., Bildsten L., 2018, ApJ, 859, L19
Bauer E. B., Bildsten L., 2019, ApJ, 872, 96
Bauer J. M. et al., 2017, AJ, 154, 53
Bear E., Soker N., 2015, MNRAS, 450, 4233
Becker J., Seligman D. Z., Adams F. C., Styczinski M. J., 2023, ApJ, 945, L24
Beust H., Vidal-Madjar A., Ferlet R., 1991, A&A, 247, 505
Biver N., Dello Russo N., Opitom C., Rubin M., 2022, preprint (arXiv:2207.04800)
Blackman J. W. et al., 2021, Nature, 598, 272
Blouin S., Xu S., 2022, MNRAS, 510, 1059
Bockelée-Morvan D., Biver N., 2017, Phil. Trans. R. Soc. A, 375, 20160252
Bodewits D. et al., 2020, Nat. Astron., 4, 867
Boe B. et al., 2019, Icarus, 333, 252
Bonsor A., Veras D., 2015, MNRAS, 454, 53
Bovy J., 2017, MNRAS, 470, 1360
Boyajian T. S. et al., 2016, MNRAS, 457, 3988
Brandner W., Zinnecker H., Kopytova T., 2021, MNRAS, 500, 3920
Brasser R., 2008, A&A, 492, 251
Brasser R., Morbidelli A., 2013, Icarus, 225, 40
Brasser R., Wang J. H., 2015, A&A, 573, A102
Brasser R., Higuchi A., Kaib N., 2010, A&A, 516, A72
Buchan A. M., Bonsor A., Shorttle O., Wade J., Harrison J., Noack L., Koester D., 2022, MNRAS, 510, 3512
Buchhave L. A., Bitsch B., Johansen A., Latham D. W., Bizzarro M., Bieryla A., Kipping D. M., 2018, ApJ, 856, 37
Caiazzo I., Heyl J. S., 2017, MNRAS, 469, 2750
Chapman C. R., 1993, Nature, 363, 492
Chayer P., 2014, MNRAS, 437, L95
Chayer P., Fontaine G., Wesemael F., 1995a, ApJS, 99, 189

Chayer P., Vennes S., Pradhan A. K., Thejll P., Beauchamp A., Fontaine G., Wesemael F., 1995b, ApJ, 454, 429
Choi J., Dotter A., Conroy C., Cantiello M., Paxton B., Johnson B. D., 2016, ApJ, 823, 102
Christensen P. R., 2006, Elements, 2, 151
Cochran A. L. et al., 2015, Space Sci. Rev., 197, 9
Collins B. F., Sari R., 2010, AJ, 140, 1306
Cordiner M. A. et al., 2020, Nat. Astron., 4, 861
Coutu S., Dufour P., Bergeron P., Blouin S., Loranger E., Allard N. F., Dunlap B. H., 2019, ApJ, 885, 74
Cunningham T., Tremblay P.-E., Freytag B., Ludwig H.-G., Koester D., 2019, MNRAS, 488, 2503
Dauphas N., 2003, Icarus, 165, 326
Dauphas N., Robert. Fran c., Bernard M., 2000, Icarus, 148, 508
Davis D. S., Richer H. B., King I. R., Anderson J., Coffey J., Fahlman G. G., Hurley J., Kalirai J. S., 2008, MNRAS, 383, L20
Dawson R. I., Murray-Clay R. A., 2013, ApJ, 767, L24
Deal M., Deheuvels S., Vauclair G., Vauclair S., Wachlin F. C., 2013, A&A, 557, L12
Debes J. H., Sigurdsson S., 2002, ApJ, 572, 556
Debes J. H., Walsh K. J., Stark C., 2012, ApJ, 747, 148
Do A., Tucker M. A., Tonry J., 2018, ApJ, 855, L10
Dones L., Weissman P. R., Levison H. F., Duncan M. J., 2004, in Johnstone D., Adams F. C., Lin D. N. C., Neufeeld D. A., Ostriker E. C., eds, ASP Conf. Series Vol. 323, Star Formation in the Interstellar Medium: In Honor of David Hollenbach. Astron. Soc. Pac., San Francisco, p. 371
Doyle A. E., Desch S. J., Young E. D., 2021, ApJ, 907, L35
Doyle A. E. et al., 2023, ApJ, 950, 17
Duncan M. J., Levison H. F., 1997, Science, 276, 1670
Duncan M., Quinn T., Tremaine S., 1987, AJ, 94, 1330
Dupuis J., Fontaine G., Pelletier C., Wesemael F., 1993, ApJS, 84, 73
Dybczyński P. A., Królikowska M., 2011, MNRAS, 416, 51
El-Badry K., Rix H.-W., 2018, MNRAS, 480, 4884
Everhart E., 1967, AJ, 72, 716
Fabrycky D., Tremaine S., 2007, ApJ, 669, 1298
Ferlet R., Hobbs L. M., Vidal-Madjar A., 1987, A&A, 185, 267
Fernandes R. B., Mulders G. D., Pascucci I., Mordasini C., Emsenhuber A., 2019, ApJ, 874, 81
Fernández J. A., 1981, MNRAS, 197, 265
Fernández J. A., 1997, Icarus, 129, 106
Fernández J. A., Brunini A., 2000, Icarus, 145, 580
Fernández J. A., Lemos P., Gallardo T., 2021, MNRAS, 508, 789
Flynn C., Holmberg J., Portinari L., Fuchs B., Jahreiß H., 2006, MNRAS, 372, 1149
Fouchard M., Froeschlé C., Valsecchi G., Rickman H., 2006, Celest. Mech. Dyn. Astron., 95, 299
Fouchard M., Froeschlé C., Rickman H., Valsecchi G. B., 2011a, Icarus, 214, 334
Fouchard M., Rickman H., Froeschlé C., Valsecchi G. B., 2011b, A&A, 535, A86
Francis P. J., 2005, ApJ, 635, 1348
Fregeau J. M., Richer H. B., Rasio F. A., Hurley J. R., 2009, ApJ, 695, L20
Frewen S. F. N., Hansen B. M. S., 2014, MNRAS, 439, 2442
Fulton B. J. et al., 2021, ApJS, 255, 14
Gaidos E., 2018, MNRAS, 477, 5692
Gaidos E., Williams J., Kraus A., 2017, Res. Notes Am. Astron. Soc., 1, 13
Gentile Fusillo N. P., Gänsicke B. T., Farihi J., Koester D., Schreiber M. R., Pala A. F., 2017, MNRAS, 468, 971
Ghezzi L., Montet B. T., Johnson J. A., 2018, ApJ, 860, 109
Hahn J. M., Malhotra R., 1999, AJ, 117, 3041
Hamilton C., Rafikov R. R., 2019, MNRAS, 488, 5489
Hamilton C., Rafikov R. R., 2021, MNRAS, 505, 4151
Harris C. R. et al., 2020, Nature, 585, 357
Heisler J., Tremaine S., 1986, Icarus, 65, 13 (HT86)
Heisler J., Tremaine S., Alcock C., 1987, Icarus, 70, 269
Heyl J., 2007, MNRAS, 381, L70
Heyl J. S., 2008a, MNRAS, 385, 231
Heyl J., 2008b, MNRAS, 390, 622
Heyl J., Penrice M., 2009, MNRAS, 397, L79
Higuchi A., Kokubo E., 2015, AJ, 150, 26
Hills J. G., 1981, AJ, 86, 1730
Hollands M. A., Gänsicke B. T., Koester D., 2018, MNRAS, 477, 93
Hoskin M. J. et al., 2020, MNRAS, 499, 171
Hughes D. W., 2001, MNRAS, 326, 515
Hunter J. D., 2007, Comput. Sci. Eng., 9, 90
Izquierdo P., Toloza O., Gänsicke B. T., Rodríguez-Gil P., Farihi J., Koester D., Guo J., Redfield S., 2021, MNRAS, 501, 4276
Izzard R. G., Dermine T., Church R. P., 2010, A&A, 523, A10
Jeans J. H., 1919, MNRAS, 79, 408
Jessberger E. K., Christoforidis A., Kissel J., 1988, Nature, 332, 691
Jewitt D., Seligman D. Z., 2022, preprint (arXiv:2209.08182)
Johnson J. A., Aller K. M., Howard A. W., Crepp J. R., 2010, Publ. Astron. Soc. Pac, 122, 905
Jones M. I. et al., 2016, A&A, 590, A38
Jura M., 2006, ApJ, 653, 613
Jura M., 2008, AJ, 135, 1785
Jura M., Young E. D., 2014, Annu. Rev. Earth Planet. Sci., 42, 45
Kaib N. A., Quinn T., 2008, Icarus, 197, 221
Kaib N. A., Quinn T., 2009, Science, 325, 1234
Kaib N. A., Volk K., 2022, preprint (arXiv:2206.00010)
Kaltenegger L., MacDonald R. J., Kozakis T., Lewis N. K., Mamajek E. E., McDowell J. C., Vanderburg A., 2020, ApJ, 901, L1
Kennedy G. M., Hope G., Hodgkin S. T., Wyatt M. C., 2019, MNRAS, 482, 5587
Kent D. V., Cramer B. S., Lanci L., Wang D., Wright J. D., Van der Voo R., 2003, Earth Planet. Sci. Lett., 211, 13
Kiefer F., Lecavelier des Étangs A., Vidal-Madjar A., Hébrard G., Bourrier V., Wilson P. A., 2017, A&A, 608, A132
Koester D., 2009, A&A, 498, 517
Koester D., Gänsicke B. T., Farihi J., 2014, A&A, 566, A34
Kostov V. B., Moore K., Tamayo D., Jayawardhana R., Rinehart S. A., 2016, ApJ, 832, 183
Kozakis T., Kaltenegger L., Hoard D. W., 2018, ApJ, 862, 69
Kral Q., Matrà L., Wyatt M. C., Kennedy G. M., 2017, MNRAS, 469, 521
Królikowska M., Dybczyński P. A., 2020, A&A, 640, A97
Lecavelier des Etangs A. et al., 2022, Sci. Rep., 12, 5855
Leto G., Jakubík M., Paulech T., Neslušan L., Dybczyński P. A., 2008, MNRAS, 391, 1350
Levine W. G., Taylor A. G., Seligman D. Z., Hoover D. J., Jedicke R., Bergner J. B., Laughlin G. P., 2023, Planet. Sci. J., 4, 20
Levison H. F., Dones L., Duncan M. J., 2001, AJ, 121, 2253
Levison H. F., Duncan M. J., Dones L., Gladman B. J., 2006, Icarus, 184, 619
Li D., Mustill A. J., Davies M. B., 2022, ApJ, 924, 61
Lin Z., Seager S., Ranjan S., Kozakis T., Kaltenegger L., 2022, ApJ, 925, L10
Liu B., Muñoz D. J., Lai D., 2015, MNRAS, 447, 747
Lodders K., 2021, Space Sci. Rev., 217, 44
McKee C. F., Parravano A., Hollenbach D. J., 2015, ApJ, 814, 13
Maldonado R. F., Villaver E., Mustill A. J., Chavez M., Bertone E., 2020, MNRAS, 499, 1854
Matrà L., Panić O., Wyatt M. C., Dent W. R. F., 2015, MNRAS, 447, 3936
Moro-Martín A., 2018, ApJ, 866, 131
Moro-Martín A., 2019, AJ, 157, 86
Muñoz D. J., Petrovich C., 2020, ApJ, 904, L3
Mullally S. E. et al., 2022, JWST Program Information, Cycle 1, ID. #1911. Space Telescope Science Institute, Baltimore. Available at: https://www.stsci.edu/jwst/science-execution/program-information?id=1911
Murray C. D., Dermott S. F., 1999, Solar System Dynamics. Cambridge Univ. Press, Cambridge, UK
Mustill A. J., Villaver E., 2012, ApJ, 761, 121
Mustill A. J., Villaver E., Veras D., Gänsicke B. T., Bonsor A., 2018, MNRAS, 476, 3939
Naoz S., Farr W. M., Lithwick Y., Rasio F. A., Teyssandier J., 2013, MNRAS, 431, 2155
Nesvorný D., Vokrouhlický D., Dones L., Levison H. F., Kaib N., Morbidelli A., 2017, ApJ, 845, 27
Novski V. et al., 2012, Cent. Bur. Electron. Telegrams, 3238, 1

O'Connor C. E., Liu B., Lai D., 2021, MNRAS, 501, 507
O'Connor C. E., Teyssandier J., Lai D., 2022, MNRAS, 513, 4178
Oort J. H., 1950, Bull. Astron. Inst. Netherlands, 11, 91
Owen T., Bar-Nun A., 1995, Icarus, 116, 215
Parriott J., Alcock C., 1998, ApJ, 501, 357
Pavlenko Y., Kulyk I., Shubina O., Vasylenko M., Dobrycheva D., Korsun P., 2022, A&A, 660, A49
Pejcha O., Antognini J. M., Shappee B. J., Thompson T. A., 2013, MNRAS, 435, 943
Petrovich C., Muñoz D. J., 2017, ApJ, 834, 116
Pichierri G., Morbidelli A., Lai D., 2017, A&A, 605, A23
Poleski R. et al., 2021, AcA, 71, 1
Portegies Zwart S., 2021, A&A, 647, A136
Rappaport S. et al., 2018, MNRAS, 474, 1453
Reffert S., Bergmann C., Quirrenbach A., Trifonov T., Künstler A., 2015, A&A, 574, A116
Rein H., Liu S. F., 2012, A&A, 537, A128
Rein H., Spiegel D. S., 2015, MNRAS, 446, 1424
Rickman H., Fouchard M., Froeschlé C., Valsecchi G. B., 2008, Celest. Mech. Dyn. Astron., 102, 111
Sanderson H., Bonsor A., Mustill A., 2022, MNRAS, 517, 5835
Schreiber M. R., Gänsicke B. T., Toloza O., Hernandez M.-S., Lagos F., 2019, ApJ, 887, L4
Seligman D. Z. et al., 2022a, PSJ, 3, 150
Seligman D. Z., Becker J., Adams F. C., Feinstein A. D., Rogers L. A., 2022b, ApJ, 933, L7
Smallwood J. L., Martin R. G., Livio M., Lubow S. H., 2018, MNRAS, 480, 57
Smallwood J. L., Martin R. G., Livio M., Veras D., 2021, MNRAS, 504, 3375
Stephan A. P., Naoz S., Zuckerman B., 2017, ApJ, 844, L16
Stephan A. P., Naoz S., Gaudi B. S., 2021, ApJ, 922, 4
Stone N., Metzger B. D., Loeb A., 2015, MNRAS, 448, 188
Strøm P. A. et al., 2020, Publ. Astron. Soc. Pac., 132, 101001
Suzuki D. et al., 2016, ApJ, 833, 145
Tamayo D., Rein H., Shi P., Hernandez D. M., 2020, Astrophysics Source Code Library, record ascl:2011.020
Teboul O., Stone N. C., Ostriker J. P., 2022, preprint (arXiv:2211.05858)
Torres S., Cai M. X., Brown A. G. A., Portegies Zwart S., 2019, A&A, 629, A139
Torres S., Naoz S., Li G., Rose S. C., 2021, MNRAS, 524, 1024
Tremblay P. E., Ludwig H. G., Freytag B., Fontaine G., Steffen M., Brassard P., 2015, ApJ, 799, 142
Tremblay P. E., Ludwig H. G., Freytag B., Koester D., Fontaine G., 2017, Mem. Soc. Astron. Italiana, 88, 104
Trierweiler I. L., Doyle A. E., Melis C., Walsh K. J., Young E. D., 2022, ApJ, 936, 30
Trierweiler I. L., Doyle A. E., Young E. D., 2023, preprint (arXiv:2306.03743)
Vanderburg A. et al., 2020, Nature, 585, 363
van Lieshout R., Kral Q., Charnoz S., Wyatt M. C., Shannon A., 2018, MNRAS, 480, 2784
Veras D., Gänsicke B. T., 2015, MNRAS, 447, 1049
Veras D., Wyatt M. C., Mustill A. J., Bonsor A., Eldridge J. J., 2011, MNRAS, 417, 2104
Veras D., Shannon A., Gänsicke B. T., 2014, MNRAS, 445, 4175
Virtanen P. et al., 2020, Nat. Methods, 17, 261
Vokrouhlický D., Nesvorný D., Dones L., 2019, AJ, 157, 181
Volk K., Malhotra R., 2008, ApJ, 687, 714
Wachlin F. C., Vauclair G., Vauclair S., Althaus L. G., 2017, A&A, 601, A13
Weissman P. R., 1996, in Rettig T., Hahn J. M., eds, ASP Conf. Ser. Vol. 107, Completing the Inventory of the Solar system. Astron. Soc. Pac., San Francisco, p. 265
Whipple F. L., 1962, AJ, 67, 1
Whipple F. L., 1978, Moon Planets, 18, 343
Wiegert P., Tremaine S., 1999, Icarus, 137, 84
Wilson T. G., Farihi J., Gänsicke B. T., Swan A., 2019, MNRAS, 487, 133
Wyatt M. C., Farihi J., Pringle J. E., Bonsor A., 2014, MNRAS, 439, 3371
Xu S., Zuckerman B., Dufour P., Young E. D., Klein B., Jura M., 2017, ApJ, 836, L7
Xu S., Dufour P., Klein B., Melis C., Monson N. N., Zuckerman B., Young E. D., Jura M. A., 2019, AJ, 158, 242
Yang B. et al. 2021, Nat. Astron., 5, 586
Zhang Y., Liu S.-F., Lin D. N. C., 2021, ApJ, 915, 91
Zieba S., Zwintz K., Kenworthy M. A., Kennedy G. M., 2019, A&A, 625, L13
Zuckerman B., Song I., 2012, ApJ, 758, 77
Zuckerman B., Young E. D., 2018, in Belmonte J. A., Deeg H., eds, Handbook of Exoplanets. Springer, Cham, p. 14
Zuckerman B., Koester D., Reid I. N., Hünsch M., 2003, ApJ, 596, 477
Zuckerman B., Koester D., Melis C., Hansen B. M., Jura M., 2007, ApJ, 671, 872
Zuckerman B., Melis C., Klein B., Koester D., Jura M., 2010, ApJ, 722, 725

This paper has been typeset from a TEX/LATEX file prepared by the author.